2012

Numerical Investigation and Performance Characteristic Mapping of an Archimedean Screw Hydroturbine

William Christopher Schleicher
Lehigh University

NUMERICAL INVESTIGATION AND PERFORMANCE CHARACTERISTIC MAPPING OF AN ARCHIMDEAN SCREW HYDROTURBINE

by

W. Chris Schleicher

A Thesis

Presented to the Graduate and Research Committee

of Lehigh University

in Candidacy for the Degree of

Master of Science

in

Mechanical Engineering

Lehigh University

November 14, 2012

This thesis is accepted and approved in partial fulfillment of the requirements for the Master of Science in Mechanical Engineering.

_____

Date Approved

_____

Dr. Alparslan Oztekin
Advisor

_____

Dr. D. Gary Harlow
Department Chair Person

TABLE OF CONTENTS

LIST OF FIGURES

Number *Page*

Number *Page*

ACKNOWLEDGMENTS

The author wishes to express sincere appreciation to Professor Alparslan Oztekin for his assistance in the preparation of this manuscript. In addition, special thanks to the Professors Garrison, Dr. Felix Flemming, Dr. Jason Faust, Michael Graft, and the Voith Hydro family in York, Pennsylvania. Your inspirations played a major role in the forming of this thesis. Also the author would like to extend a special thanks and appreciation to Robert Kline. Without his efforts, this thesis would not have been possible.

NOMENCLATURE

t	Time [s]	ϱ	Density [kg m^{-3}]	k	Turbulent Kinetic Energy []
u	Velocity [m s^{-1}]	μ	Local Dynamic Viscosity [kg m^{-1} s^{-1}]	μ_t	Turbulent Viscosity [kg m^{-1} s^{-1}]
σ_k	Constant [1.0]	P_k	Production of k	ε	Turbulent Dissipation [ ]
σ_ε	Constant [1.3]	$C_{1\varepsilon}$	Constant [1.42]	$C^*_{2\varepsilon}$	Constant [ ]
$C_{2\varepsilon}$	Constant [1.68]	C_μ	Constant [0.0845]	η	Constant [ ]
η_0	Constant [4.8]	β	Constant [0.012]	S	Modulus of the mean rate-of-strain tensor
S_{ij}	Rate-of-strain tensor	$\overline{u}$	Average Local Velocity [m s^{-1}]	u_{avg}	Average Velocity [m s^{-1}]
I	Turbulent Intensity [ ]	l	Characteristic Length [m]	D_H	Hydraulic Diameter [m]
u_P	Mean Velocity of the Fluid at the Near-wall node P [m s^{-1}]	U^*	Friction Velocity [m s^{-1}]	τ_w	Wall Shear Stress [kg m^{-1} s^{-2}]
ΔB	Parametric Constant [ ]	E	Empirical Constant [9.793]	y_p	Distance to the Wall from the Adjacent Cell Centroid [m]
$\varkappa$	Von Kármán Constant	f_r	Roughness Function [ ]	$\Delta H_{turb.}$	Calculated Turbine Head [m]
$P_{turb.}$	Calculated Turbine Power [W]	$\eta_{turb.}$	Calculated Turbine Efficiency [%]	$\Delta P_{Stat.+Dynam.}$	Change in Stat. and Dynam. Pressure [Pa]
ϱ_w	Density of Water [kg m^{-3}]	τ_{blade}	Torque on the Turbine Blade [N m]	Ω_{blade}	Rotation Rate of the Blade [rad s^{-1}]
Q	Volumetric Flow Rate [m^3 s^{-1}]	X	x-coordinate [m]	Y	y-coordinate [m]
Z	z-coordinate [m]	t	Parametric Variable [ ]	N	Number of Blade Rotations [ ]
m	Constant [1.5]	L	Shaft Length [0.4953 m]	l_{shaft}	Current Location Along the Shaft Length [m]

ABSTRACT

Computational Fluid Dynamics (CFD) is a crucial tool in the design and analysis of hydraulic machinery, especially in the design of a micro hydro turbine. The micro hydro turbine in question is for a low head (less than 60 meters), low volumetric flow rate (0.005 m^3/s to 0.5 m^3/s) application with rotation rates varying from 200 RPM to 1500 RPM. The design of the runner geometry is discussed, specifically a non-uniform Archimedean Spiral with an outer diameter of 6 inches and length of 19.5 inches. The transient simulation method, making use of a frame of reference change and a rotating mesh between time-steps, is explained as well as the corresponding boundary conditions. Both simulation methods are compared and are determined to produce similar results. The rotating frame of reference method was determined to be the most suitable method for the mapping of performance characteristic such as required head, torque, power, and efficiency. Results of simulations for a non-uniform Archimedean Spiral are then presented. First, a spectral and temporal convergence study is conducted to make sure that the results are independent of time-step and mesh selection. Performance characteristics of a non-uniform pitched blade turbine are determined for a wide range of volumetric flow rates and rotation rates. The maximum efficiency of the turbine is calculated around 72% for the design of the turbine blade considered in the present study.

Chapter 1

INTRODUCTION

Harnessing the power of flowing water has been done for many millennia, with examples dating back 2000 years ago in China and Greece where the water wheel was used to grind wheat into flour [1] [2]. Today, hydropower is used to supply the world with 20 percent its electricity needs [3].

Hydropower has a long history within the United States. Niagra Falls was the first location in the United States where a hydroelectric plant was installed, but it was not until after World War I that hydroelectric plant design became standardized [2]. In this time, about 40 percent of the United States power generation came from these hydroelectric plants, however, today hydropower provides about six percent of the United States' electricity [2].

Clean, renewable energy is a hot topic in the modern power generation field. Hydropower is a perfect means to fulfill these two requirements. Hydropower is renewable because it relies on natural precipitation cycles and is clean because it produces no air pollution. A hydroelectric facility can take many forms: using a reservoir, using channels to redirect flow from a river, or a pump storage facility using an upper and lower reservoir [4]. The majority of the arguments against hydropower are environmental and aesthetic in nature. Constructing a reservoir can affect the oxygen levels downstream of the reservoir and can affect the plant, aquatic and nearby habitats of land-dwelling animals for example [4]. Large scale hydropower, defined by the U. S. Department of Energy as a facility that can produce more than thirty megawatts of power, also has high capital costs [4].

Micro-hydro applications are an excellent way to address these negative issues of large scale hydropower. Micro-hydro is a small scale application of these larger units and has the advantage that it can work with the surrounding environment with little impact. More specifically, a hydrokinetic application would suite these needs well. A hydrokinetic application would allow the turbine to be submerged in a moving stream and make use of the current to generate electricity. This application would not require the use of a reservoir or a diversion in the river, which makes this application more environmentally friendly.

Hydrokinetic micro-hydropower generation would be excellent for farming or remote places. This application would have a direct benefit in rural areas by producing revenue to repay irrigation facilities and providing power for other farming or domestic purposes [2]. For remote locations, hydropower can even be a cheaper alternative than having power lines brought to the location from the main power grid. It may take a few years to pay off the capital investment for these micro hydro installations, but once the system is paid off the installation will begin to net profit.

This thesis will focus mainly on the design, simulation, and characterization of a non-uniform pitch Archimedes screw. It will discuss the flow regime that is developed by this turbine. Different simulation methods will be introduced and compared.

HYDRO TURBINE CLASSIFICATION

There are two primary classifications of hydro turbines: reaction and impulse turbines. Reaction turbines are fully immersed in water and rely on a pressure difference across the

blade passages to spin the turbine. An impulse turbine is not immersed and converts the high pressure upstream of the turbine to a fast jet that strikes the turbine buckets, turning the turbine.

The type of turbine that is appropriate for a specific application is dependent on the available head and flow rates seen by the turbine. The available head will determine the shape of the turbine, while the flow rate will determine the size of the turbine [3].With head and flow rate known, there are three basic hydro turbine designs that are commonly used today: Pelton, Francis, and Kaplan turbines.

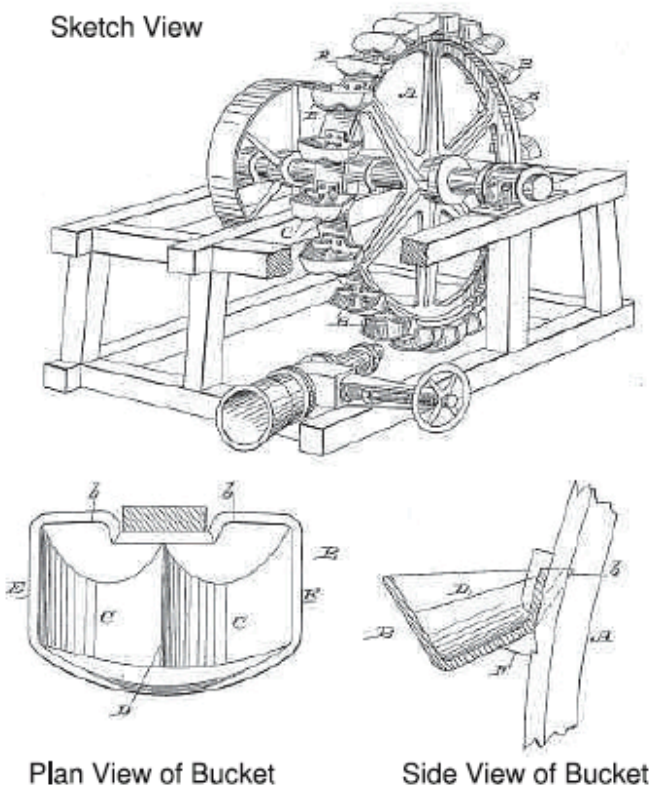

Figure 1: Schematic of Lester Pelton's Patent [3]

The Pelton Wheel was invented by Lester Pelton around 1880 [3]. A schematic of this design is pictured in Figure 1. This design makes use of a high head (around 300 to 400 meters) to channel fluid into one to three nozzles that spray onto bucks on the rotor [3]. The buckets then deflect the flow ideally 180 degrees from its inlet direction which allows for the rotor to turn. A Pelton turbine is therefore classified as an impulse machine and has peak efficiencies around 90% [3].

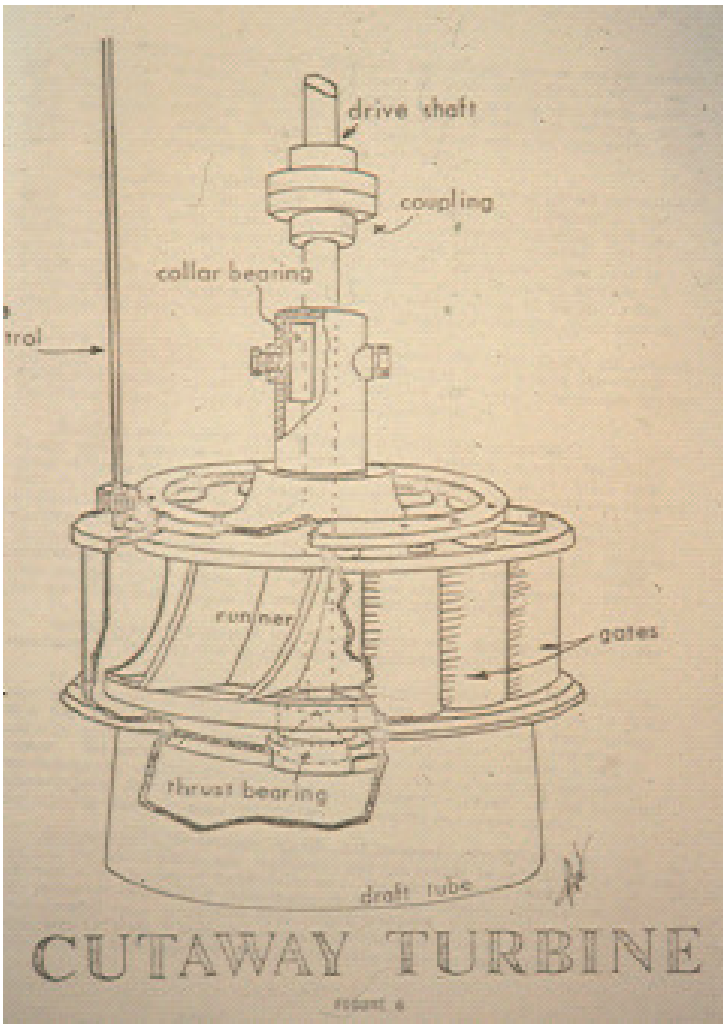

Figure 2: Original Schematic of a Francis Turbine [5]

The Francis turbine was invented by James B. Francis around the mid 1850's [5]. He was looking at reinventing a waterwheel and discovered that by turning it on its side and making a few other modifications, he could increase the wheel's efficiency from around 65% to about 88% [5]. The application for a Francis turbine is in a "moderate" range of head [3]. Figure 2 is an original schematic of a Francis turbine. Key features to a Francis turbine are the volute or spiral case, stationary guides called stay vanes, rotatable guides called wicket gates, and the Francis runner itself. This machine is considered as a reaction turbine.

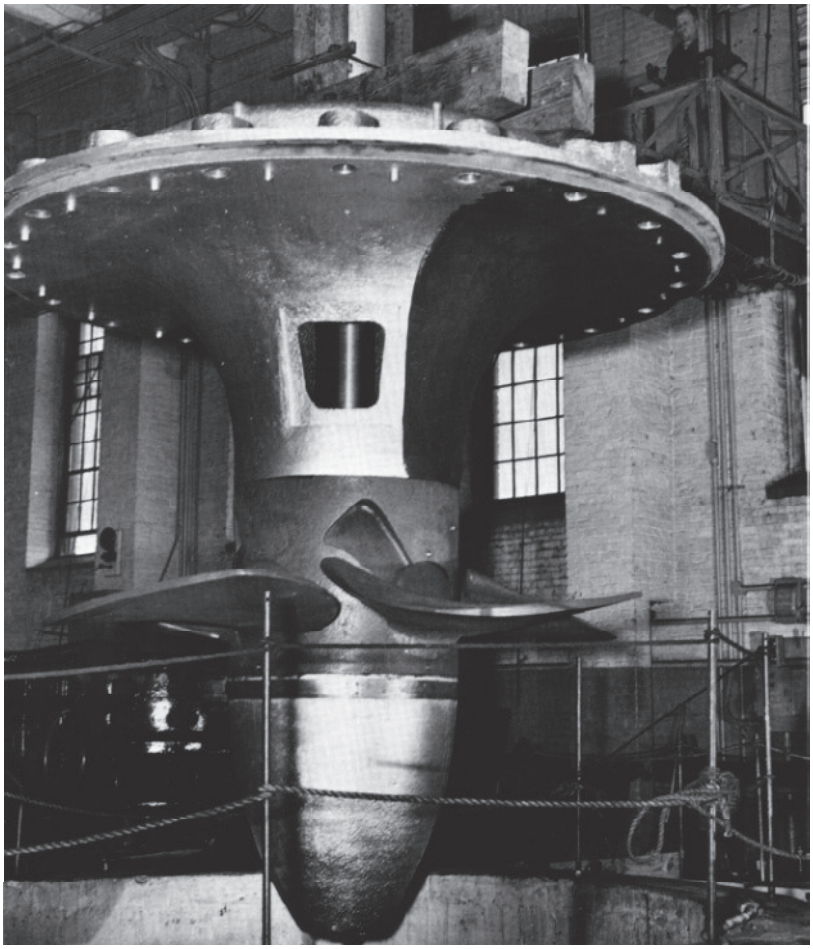

Figure 3: Example of a Typical Kapln Turbine [6]

Finally the Kaplan was designed by Viktor Kaplan around 1929 [6]. This machine is noted for its high efficiency over a wide range of operation [6]. Components of a Kaplan turbine can be very similar to that of a Francis turbine, with the exception that a Kaplan turbine operates axially rather than radially [3]. Some units even avoid the hassle of converting the radial flow to an axial flow all together and are strictly axial machines such as a bulb turbine [3]. Figure 3 is an example of a typical Kaplan turbine.

THE COMPUTATIONAL FLUID DYNAMICS METHODOLOGY

Computational Fluid Dynamics (CFD) is a tool widely used in industry today, and has it's developing roots back in the 1950's and 1960's for trying to solve for the flow over blunt bodies at supersonic speeds [7]. This problem was of interest because of ICBM's and later the space program and perplexed many scholars of the time. Today this problem has been reduced to a mere homework assignment for students studying fluid mechanics. This goes to show the progress that has been made in the past half century in this field has made remarkable leaps in how these numerical methods help scientists and engineers solve practical problems for our time.

There is a set methodology behind planning and implementing a CFD solution. This being geometry creation, grid generation, choosing appropriate models, supplying appropriate boundary conditions, finding an appropriate solution to the governing equations and boundary conditions, and post-processing the results of the computation. These six basic steps are common in any CFD problem no matter what is to be studied.

Geometry generation is usually carried out by Computer Aided Design (CAD) or 3D modeling package. Attention has to be made to simplifying the geometry so that a satisfactory grid can be generated in the next step. Features such as fillets or very small clearances relative to the size of the computational domain are usually neglected at this time because their presence usually has little effect on the calculated flow field or the computational resources required to model these features outweigh what is available. In regards to turbo-machinery objects such as fillets of the blades to the hub, a requirement for the structural integrity of the runner, are usually ignored at this stage. Also, the clearance between the runner blade and the shroud, usually on a scale of a couple millimeters as compared to a few meters in diameter for the runner itself, is not modeled due to computational limitations.

In the next phase, a grid or mesh is generated from the input geometry. There are several considerations that must be taken into account in what will make up the grid. Foremost, the kind of grid must be chosen such as a structured, block structured, unstructured, or hybrid grid based on factors such as personal experience, computational limitations, and how sensitive the solution is to the implementation of the chosen grid [7]. Other considerations are if the solution is viscous, then a mesh resolving the boundary layer must be considered or if the solution is turbulent, then appropriate first cell layer Yplus values should be met.

Following grid generation, the appropriate models must be chosen for the problem at hand. Questions such as must the solution be in 3D or can it be simplified to a 2D problem without sacrificing too much accuracy to the results need to be determined. It should also be known if the problem is a steady-state or transient in nature. Will an incompressible continuum assumption be valid? If not, will heat transfer play an important role in a

compressible scenario? Is the flow laminar, turbulent, or even both? These are just some of the major principles that must be thought of carefully at this point in this methodical process. There are other considerations too, such as if the flow is multiphase, contains a chemical reaction, or if there is a movement in the geometry involved [7].

Once an appropriate model is chosen for the goals of the simulation, the boundary conditions are supplied. Control volume principles such as inlets and outlets of the overall computational domain are specified with parameters such as velocities, static pressures, mass flow rates, temperatures, and turbulence conditions. Walls of the domain are also specified and are given conditions such as if they are rotating or translating in space, if they are ideal no-slip walls or have a specified wall roughness, and if a specified shear stress is applied by the working fluid on the wall. Periodic boundary conditions can be supplied when a fluid particle leaves one surface of the computational domain and reenters the domain on a specified surface. Such a boundary condition is a useful approximation in turbo-machinery allowing only a single blade or guide vane to be numerically modeled instead of the entire cascade. Finally, interfaces between computational domains can be specified for solutions requiring multiple reference frames where the results at a boundary for one domain can be interpolated onto a coexisting boundary. This can increase the complexity of the solution, but at the same time allow for a more stable and accurate solution if implemented correctly.

At this point, a solution is ready to be calculated. Writing homemade code is a possibility, but today there are many commercially available (CFX, Fluent, STAR-CD, etc.) and open-source codes (OpenFOAM) where a solution can be calculated. Input parameters such as the number of maximum iterations or in the case of a transient problem, the number of time-steps, time-step size, and maximum iterations per time-step must be supplied. One

cannot just simply run the calculation and wait for a final result, close monitoring of the solution is usually required for the computational fluid dynamics simulations of complex geometries such as the one considered in this work. Plots such as the RMS or maximum cell residuals between calculations for each equation solved in each outer iteration of the solution should be monitored for values approaching zero. If the residuals are zero, this means that the calculated value between iterations has not changed thus a solution may have converged. A solution may have converged and not definitely converged because along with residuals, key performance characteristics based on the goals of the calculation should be monitored for convergence on a reasonable value.

Finally, once the solution is determined to be converged, the fruits of the labor can be reaped from post-processing the calculated solution. Here streamlines, contours, velocity vectors, and other fascinating features can be impressively calculated and displayed with ease. Here though it takes a person familiar both with the problem at hand and the numerical methods used to derive the solution to determine if this result makes physical sense. If in any of the previous steps an improper assumption or implementation of a model or boundary condition is applied, the post-processed results are nothing more than impressive figures of conditions that do not make any physical sense.

Chapter 2

DESIGN AND MESHING

Previously mentioned were the various types of standard hydro turbine designs and their general application. This investigation was focused on a low head, low volumetric flow rate application of a hydro turbine. Another important requirement was the portability of this device. This hydro turbine must be easy to transport and set-up by a small team in as little time possible. Finally, the turbine should have a hydrokinetic application as well. This paper will focus on the run-of-river setup, where a head of water would be developed by diverging water from a river through a penstock.

The design chosen to accomplish this task is not a standardized design. A twist on the Archimedean screw was adapted where the pitch of the screw changed as a function of shaft length. At the leading edge, the pitch is steep and then transitions to almost perpendicular pitch to the flow direction at the trailing edge. The idea behind this design is to be able to have more control of the pressure difference between the pressure side and suction side of the blades, allowing for more torque to be extracted from the fluid as opposed to a more traditional uniformly pitched Archimedean screw.

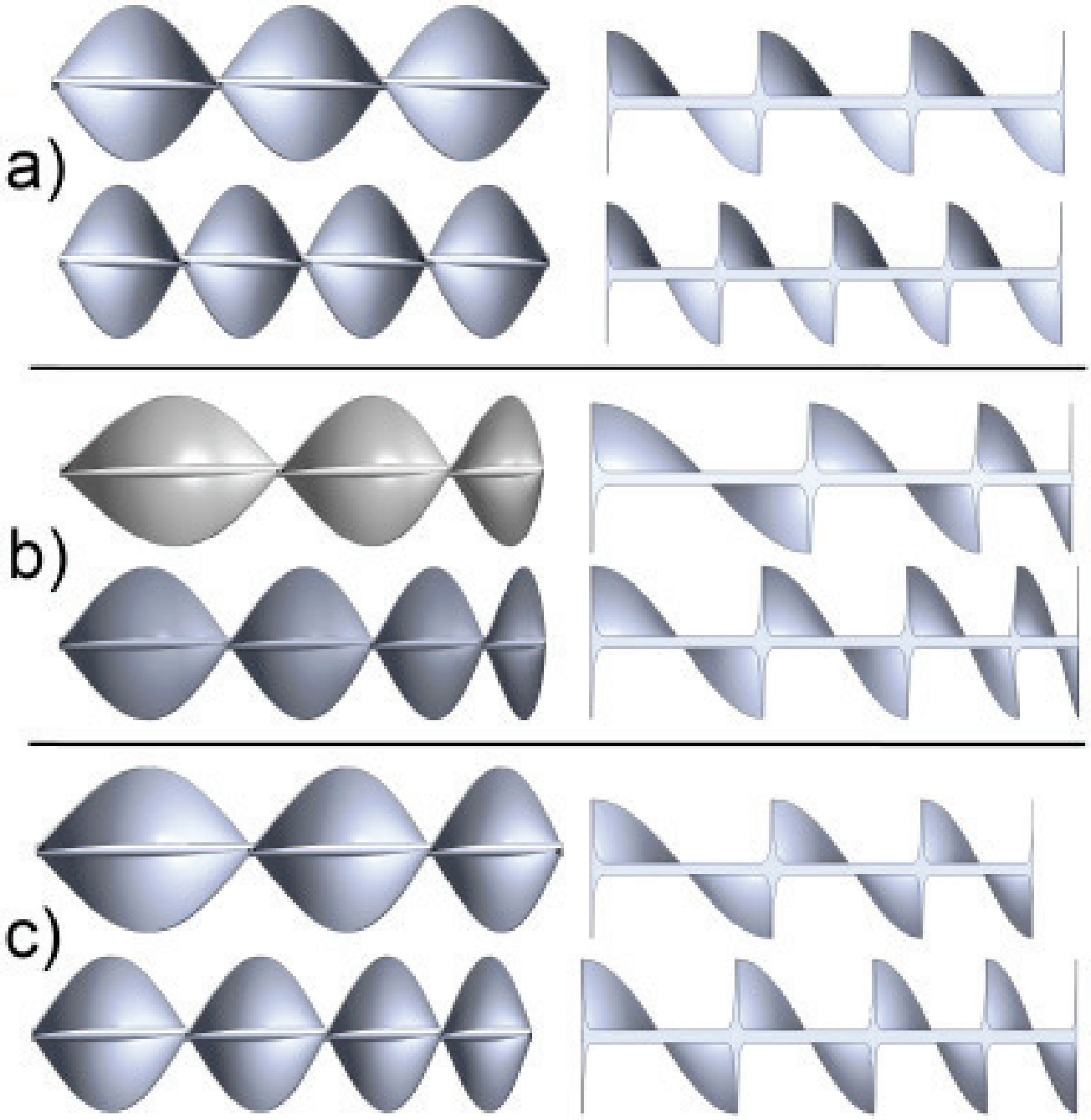

Figure 4: a) Uniformly Pitched Blades, b) Non-uniformly pitched blades based on a Power Relationship, c) Non-uniformly Pitched Blades Based on an Arctangent Relationship

Pictured in Figure 4 are some examples of geometries that were investigated for this application. Figure 4a represents a standard Archimedean screw that has uniform pitch from leading to trailing edges. Figure 4b and c represent the non-uniformly pitched Archimedean screws that were investigated. The pitches of these screws are governed by equations 1 and 2. Figure 4b represents the power relationship shown in equation 1. Figure 4c uses similar equations with the exception of the z-coordinate which is shown in equation 2.

$$\begin{matrix} X \\ = R\cos(t) \end{matrix} \quad \begin{matrix} Y \\ = R\sin(t) \end{matrix} \quad Z = L\left(1 - \left(\frac{t}{N\pi}\right)^m\right) \quad t = l_{shaft}\frac{N\pi}{L} \qquad \textbf{(1)}$$

$$Z = L\left(1 - \frac{\operatorname{atan}\left(\frac{t}{N\pi}\right)}{\operatorname{atan}(1)}\right) \qquad \textbf{(2)}$$

In these equations, X, Y and Z are the coordinate locations of the point in question, R is the radius of the blade, L is the shaft length, l_{shaft} is the current location along the shaft's length, N is the number of wrapping turns the blade makes around the shaft, m is a specified constant, and t is a parametric variable.

These equations were used in a MATLAB script to export points to a text file. This text file was then imported into the CAD package SolidWorks to create splines that would govern the geometry of the blades of the screw. A shaft was also added to the geometry at this stage and once complete, the geometry was exported for numerical investigation.

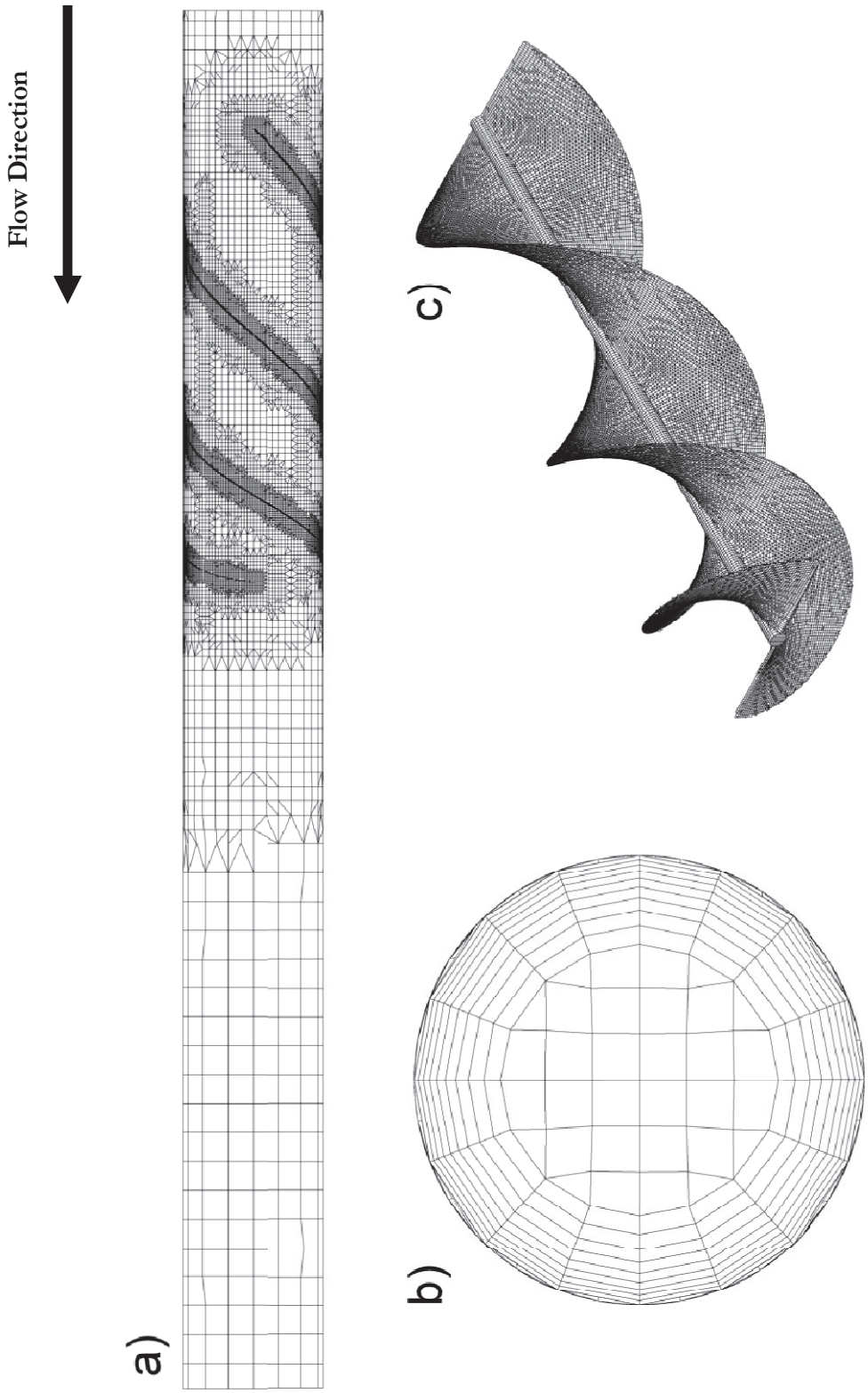

Figure 5: Example Domain and Mesh Used in the Investigation a) The Entire domain b) Cross-sectional View from the Outlet c) Surface Mesh on the Turbine Blade

First, before a mesh can be generated the size of the computational domain must be determined. In the run-of-river design method, water would be diverted from a body of water through a hose, pass through the turbine, and be reintroduced into another body of water. The domain for a CFD calculation of this method makes sense to include the screw housed in a pipe approximately the diameter of the turbine. Figure 5 depicts the schematic of the flow problem. The turbine, which has a hydraulic diameter of six inches and shaft length of 19.5 inches, has been placed inside a housing. This housing is a simple pipe with a hydraulic diameter of six inches and length of 63.5 inches. For these simulations, therefore, the gap between the blade and the housing is not modeled. Figure 5a depicts the entire computational domain. Figure 5b is a cross section of the mesh on the outlet face and Figure 5c shows the surface mesh on the turbine blade itself.

The accuracy of results produced through a CFD calculation is only as good as the mesh that is provided for analysis [8]. There are a few basic meshing techniques such as a structured or unstructured mesh and the mesh can be comprised of different element types. The most common element types are hexahedra, tetrahedral, square pyramids and extruded triangles. Unstructured 3D grids tend to use hexahedra and tetrahedral elements, while structured grids rely more on quadrilateral and hexahedral elements [9].

The mesh used makes use of a few different elements. The base element that comprised the mesh is a hexahedral element. Tetrahedral elements were also used to help bridge the gap between hexahedral elements when the boundaries could not be resolved well. In order to resolve the boundary layer, prism elements were used by inflating the size of the

element by 1.2 times the original prism size to help transition the boundary mesh to the main hexahedral mesh.

Attention had to be made with the element sizes used in the mesh. Using smaller elements can improve the accuracy of the solution, but will require more computational resources and time to generate the solution. Using larger elements eases the computational requirements of the calculation, but the results may not be as accurate. Therefore, a balance between using larger and smaller elements needs to be implemented. Smaller elements should be used in regions of interest and near wall and larger elements should be placed in regions of less importance to the solution. A spectral investigation on the effect of mesh element size on the solution will be presented later in this paper.

Chapter 3

MODELING AND NUMERICAL METHOD

Computational Fluid Dynamics plays a vital role in the design of turbo-machinery. This tool allows for multiple design iterations in a considerably shorter amount of time than having to construct a model and running an experiment. With computational power increasing over the years, this tool becomes an even more robust analysis method. Even though this tool provides the possibility of a more productive analysis method, the results obtained from a simulation are only as good as the information in which is provided to the program. The tool has the capability of producing some impressive colorful images, but if the data or method provided to the simulation does not have a physical representation, pretty colorful images are all the results obtained are good for. Experience and physical data will lead to more meaningful, physical results from this analysis.

Turbo-machinery provides and interesting application for CFD. In the real world, an impeller is rotating about a central axis at a certain angular speed due to the interaction between the working fluid and the impeller. This makes meshing in the area near the impeller an interesting task. Careful thought should be taken into consideration on how to deal with this. Since the impeller is rotating, this makes the fluid flow in this region transient in nature. There are two schools of thought to modeling this transient nature. The first is to rotate the mesh in the region of the impeller at an angular speed equal to the rotation rate of the impeller, thus computational mimicking the motion of the physical phenomenon of the impeller. The second is to not rotate the mesh itself, but to rotate the frame of reference in the region near

the impeller at an angular speed equal to that of the impeller rotation rate. This allows for a relative calculation of the flow parameters to this rotating reference frame. The goals of both these methods are the same, but each has their advantages and disadvantages in modeling the phenomenon in the region near the impeller.

The method that was ultimately settled on to accomplish modeling the transient nature of the flow near the impeller was using the frame of reference change. The velocity field was formulated relative to the rotating frame of reference, and thus two additional terms are added to the conservation of momentum equation representing the Coriolis and centripetal accelerations [10]. Equations for conservation of mass and conservation of momentum take the following form:

$$\frac{\partial \rho}{\partial t} + \nabla \cdot \rho \vec{v}_r = 0 \tag{3}$$

$$\frac{\partial}{\partial t}(\rho \vec{v}_r) + \nabla \cdot (\rho \vec{v}_r \vec{v}_r) + \rho(2\vec{\omega} \times \vec{v}_r + \vec{\omega} \times \vec{\omega} \times \vec{r}) = -\nabla p + \nabla \cdot \bar{\bar{\tau}}_r + \vec{F} \tag{4}$$

Here $\vec{v}_r$ is the relative velocity vector of the fluid, ρ is the fluid density, ω is the angular velocity vector, P is the pressure, $\bar{\bar{\tau}}_r$ is the shear stress tensor, $\vec{F}$ is the external applied force, t is the time, and ∇ is the differential vector operator.

Another computational feat that must be accomplished is in modeling turbulent structures in the flow field. These turbulent structures occur on many different length and time scales, making modeling all possible length and time scales a computational task that is beyond practical. There are a few different turbulence models available to accomplish capturing the

important turbulent length and time scales. The model that was used in this study is a variant on the standard k-epsilon model called the renormalized group k-epsilon model.

The renormalized group analysis of turbulence was first investigated by Yakhot and Orszag [11] in 1986, and a turbulence model was developed later in 1992 that offers improvement in modeling turbulence at high Reynolds numbers by removing the smallest scales of turbulence, allowing computation of these turbulence scales a more feasible task [12]. The transport equations are for this method area as follows:

$$\frac{\partial}{\partial t}(\rho k) + \frac{\partial}{\partial x_i}(\rho k u_i) = \frac{\partial}{\partial x_j}\left[\left(\mu + \frac{\mu_t}{\sigma_k}\right)\frac{\partial k}{\partial x_j}\right] + P_k - \rho\varepsilon \tag{5}$$

$$\frac{\partial}{\partial t}(\rho\varepsilon) + \frac{\partial}{\partial x_i}(\rho\varepsilon u_i) = \frac{\partial}{\partial x_j}\left[\left(\mu + \frac{\mu_t}{\sigma_\varepsilon}\right)\frac{\partial \varepsilon}{\partial x_j}\right] + C_{1\varepsilon}\frac{\varepsilon}{k}P_k - C_{2\varepsilon}^{*}\rho\frac{\varepsilon^2}{k} \tag{6}$$

$$C_{2\varepsilon}^{*} = C_{2\varepsilon} + \frac{C_\mu \eta^3(1-\eta/\eta_0)}{1+\beta\eta^3} \tag{7}$$

$$\eta = S\frac{k}{\varepsilon} \qquad S = \left(2S_{ij}S_{ij}\right)^{1/2} \qquad \mu_t = \rho C_\mu \frac{k^2}{\varepsilon} \tag{8}$$

In the above equations, ϱ is the fluid density, μ is the local dynamic viscosity, μ_t is the turbulent viscosity, P is the pressure, k is the turbulent kinetic energy, ε is the turbulent energy dissipation, t is the time, x is a position vector, u is a velocity vector, C_μ, $C_{1\varepsilon}$, $C_{2\varepsilon}$, σ_k and σ_ε are prescribed constants, $C_{2\epsilon}^{*}$ and η are parametric constants, S is the modulus of the mean rate-of-strain tensor, S_{ij} is the rate of strain tensor and the small script i, j and k are vector integers. In

these equations, the buoyancy terms have been neglected. The constants used in these calculations for C_{μ}, $C_{1\varepsilon}$, and $C_{2\varepsilon}$ are 0.0845, 1.42 and 1.68, respectively.

Boundary conditions play an important role in the accuracy of solutions as well. At the inlet to the computational domain, a fully-developed turbulent velocity profile was assumed. The turbine is encased in a pipe-like housing, thus a standard empirical relationship that governs the velocity profile is given by:

$$\frac{\overline{u}}{U} = \left(1 - \frac{r}{R}\right)^{1/n} \quad \textbf{(9)}$$

$$n = -1.7 + 1.8 ln Re_U \quad \textbf{(10)}$$

Here $\bar{u}$ is the average local velocity, U is the maximum velocity, r is the local radius, R is the total outer radius, n is a parametric constant, and Re_U is Reynolds number using the maximum velocity at the characteristic velocity and the pipe diameter as the characteristic length. In this relationship, the ratio of the local velocity to the maximum velocity is defined by the percent distance from the outer radius of the pipe raised to the inverse an empirical exponent.

On the inlet and outlet of the domain, parameters of turbulence are defined for turbulence kinetic energy and turbulent dissipation rate. These parameters were back calculated through the input parameters of a specified turbulent intensity and hydraulic diameter. These parameters, I and $D_{H,}$ were 10% and 0.1524 m, respectively. Ten percent for turbulent intensity represents a pretty turbulent condition based on a professional opinion. The hydraulic

diameter is just the diameter of the encasing. This value is used to determine the length scale used in the k and epsilon parameters by $l = 0.07\ D_H$. The turbulent kinetic energy and dissipation rate can then be calculated by:

$$k = \frac{3}{2}\left(u_{avg} I\right)^2 \quad \textbf{(11)}$$

$$\varepsilon = C_\mu^{3/4} \frac{k^{3/2}}{l} \quad \textbf{(12)}$$

Here k is the turbulent kinetic energy, ε is the turbulent energy dissipation, u_{avg} is the average velocity, I is the turbulent intensity, l is a characteristic length scale, and C_μ is a prescribed constant. These relationships for the turbulence model were used both on the inlet and outlet faces of the domain. The specified values for the turbulent intensity (I) and hydraulic diameter (D_H) were 10% and 0.1524 m, respectively.

The turbine is encased in a housing that has a no-slip condition applied to it, and is assumed to have hydraulically smooth walls. A modified equation for the law-of-the-wall is used to calculate the shear stress acting on the wall [13].

$$\frac{u_p u^*}{\tau_w/\rho} = \frac{1}{\kappa} ln\left(E \frac{\rho u^* y_p}{\mu}\right) - \Delta B \quad \textbf{(13)}$$

$$u^* = C_\mu^{1/4} k^{1/2} \qquad \Delta B = \frac{1}{\kappa} ln(f_r) \quad \textbf{(14)}$$

In these equations, u_p is the mean velocity of the fluid at the near-wall node p, u^* is the friction velocity, τ_w is the wall shear stress, ϱ is the fluid density, ϰ is the Von Kármán constant, E is an empirical constant, y_p is the distance to the wall from the adjacent cell centroid, μ is the

dynamic viscosity, ΔB is a parametric constant, C_μ is a prescribed constant, k is the turbulent kinetic energy, and f_r is a roughness function. Since the assumption of hydraulically smooth walls is in effect, however, these equations are not evaluated in the simulations as a boundary condition.

Chapter 4

RESULTS AND DISCUSSION

A study was conducted to optimize the mesh, computational domain, and time-step selection for a transient CFD analysis. Such studies are common in the numerical world to prove spectral and temporal convergence of the solution [14] [15]. The domain inlet boundary condition was placed five inches away from the leading edge of the impeller, and outlet boundary condition was placed approximately fifteen inches away from the trailing edge. The additional length at the outlet was to ensure that the outlet boundary condition had little computational effect on the solution in the region of the runner. Three different meshes were used, ranging from coarse to fine, in order to determine the effect the mesh had on the calculated solution. The general size of the mesh elements and refinement near solid to fluid interfaces was varied to determine how the mesh influences the calculation of performance characteristics for the turbine. Three different meshes were used: a coarse mesh containing approximately eight hundred thousand elements, a medium mesh with approximately two million elements, and a fine mesh made up of approximately four million elements. These meshes were built around the same turbine geometry, with the same boundary conditions applied to each mesh.

The head calculated from the simulations, as a function of time, can be seen in Figure 6. The corresponding power generated from the interaction between the flow and the turbine blade is displayed in Figure 7. Based on the flow rate, the head, and the torque generated, efficiency was determined and is shown in Figure 8. In Figure 6 through Figure 8, an initial

spike in the value is observed with the values settling around a given value as the turbine reaches steady state. Table 1 shows the maximum, minimum, and average Yplus value along the blade for each simulation done. Table 2 displays the maximum, minimum, and average Yplus values, much like Table 1, only for the housing/wall of the fluid.

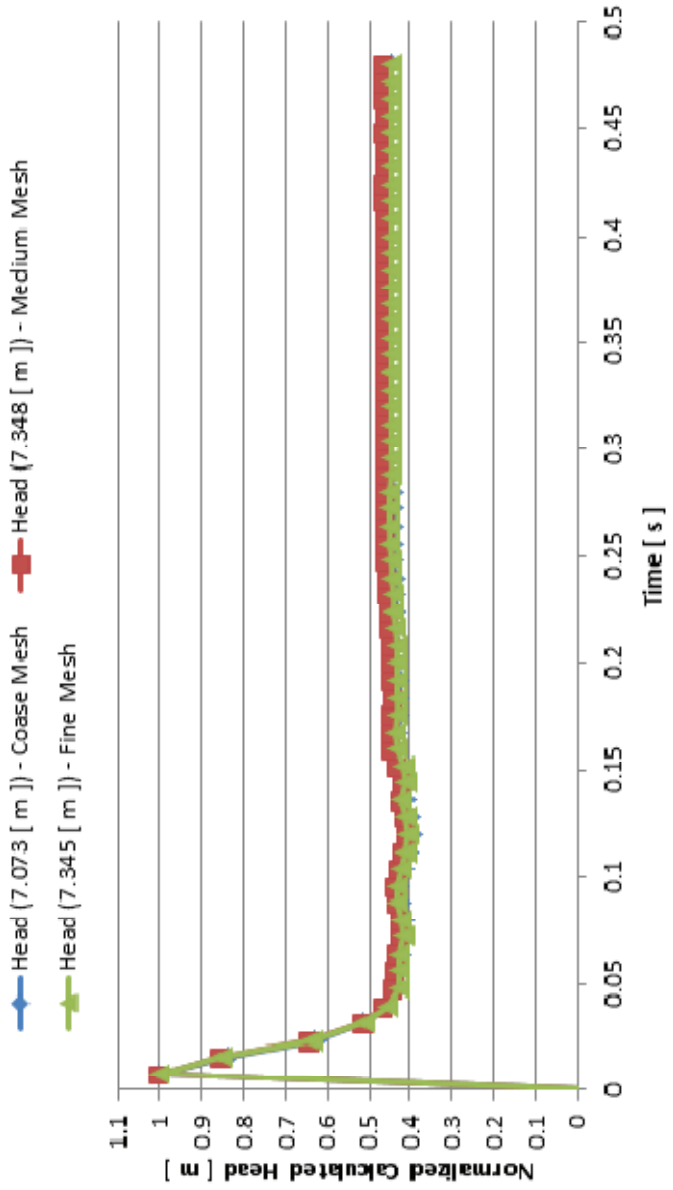

Figure 6: Normalized Head over Time

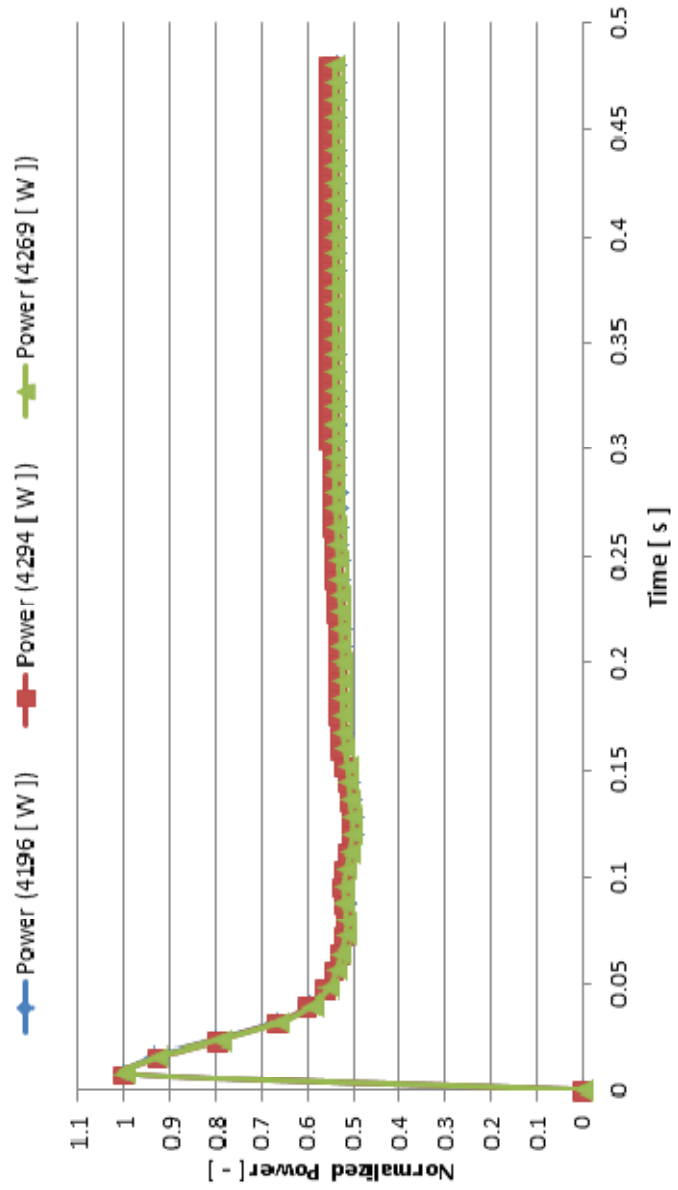

Figure 7: Normalized Power over Time

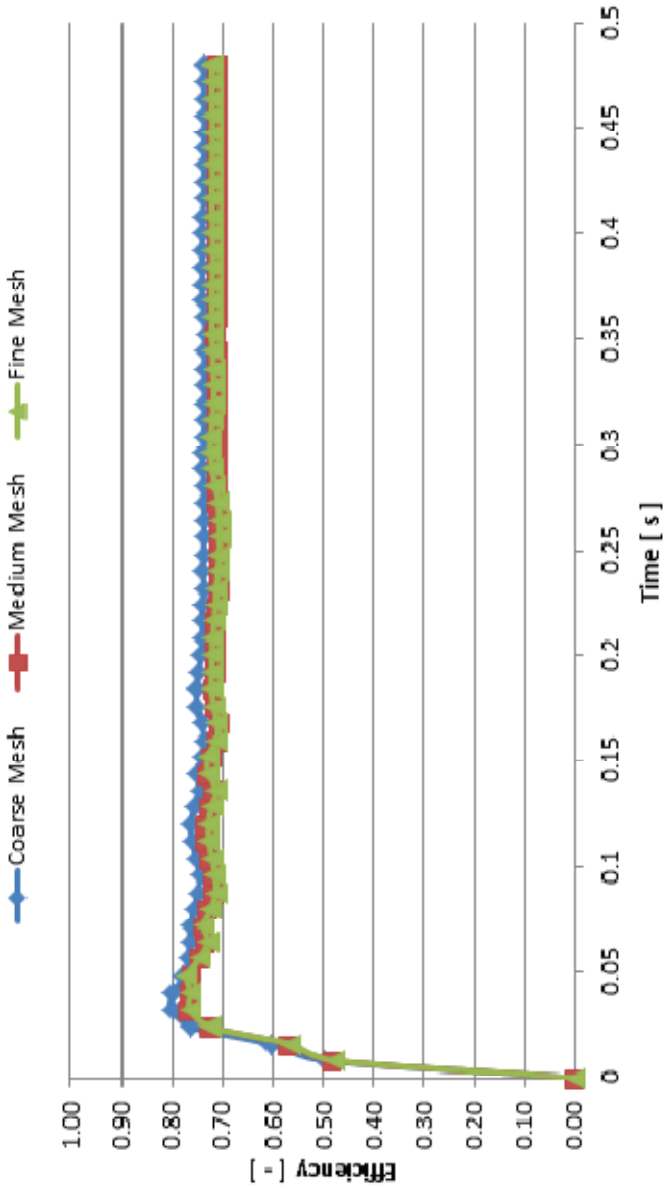

Figure 8: Normalized Efficiency over Time

Table 1: First Layer Yplus Values on the Blade

	Coarse Mesh	Medium Mesh	Fine Mesh
Min Yplus (Blade)	1.112	1.879	1.338
Max Yplus (Blade)	223.464	120.86	65.728
Avg Yplus (Blade)	60.614	27.977	18.989

Table 2: First Layer Yplus Values on the Housing

	Coarse Mesh	Medium Mesh	Fine Mesh
Min Yplus (Housing)	3.411	15.463	8.234
Max Yplus (Housing)	145.207	72.982	40.64
Avg Yplus (Housing)	93.997	52.014	25.794

The result of head versus time, as seen in Figure 6, shows that the meshes produce a pseudo-steady-state solution around a time of 0.25 seconds. The trade-off between meshes from the perspective of calculated head is that a coarse mesh will tend to converge on a pseudo-steady result quicker, but over predict the value of head. A finer mesh will suggest a more accurate range of head, but will take more computational time and resources to settle on a value if even at all. The medium mesh appears to be a good compromise between the two trade-offs.

From the plot of calculated power versus time, seen in Figure 7, a similar trend can be observed as in the results of head versus time. The coarse and fine meshes appear to agree on the same pseudo-steady-state value for power, while the medium mesh predicts a value slightly

higher than the two. Calculated efficiency versus time is dependent upon the solutions of both head and power. The interaction between these two calculated values can be seen in Figure 8.

The first layer Yplus values, as shown in Tables 1 and 2, for the three meshes also offer insight as to why the calculated operating parameters produced the given results. On the coarse mesh, the Yplus values were fair around the blade; however, around the housing the Yplus values are inappropriate for proper boundary layer resolution. This can explain why the coarse mesh tended to settle on operating parameters and over predict them compared to the finer meshes. The results show that the element size of the medium mesh is appropriate as a compromise between computational time and resources and the accuracy of the results. Special attention should be paid to resolving the boundary layer near the solid-fluid interface to be sure that a more physical result is obtained.

THE ROTATING MESH METHOD

As mentioned earlier, there were two methods investigated to attempt to capture the transient nature of the rotating impeller within the computational domain. The first method that was investigated was using a rotating mesh, where the mesh rotated at the same angular speed of the turbine. The following results are for a volumetric flow of 0.1 m^3/s with a rotation rate of 750 RPM. The results for the rotating mesh method will be displayed first, followed by the results from the frame of reference method and a comparison between the two results. Figure 9 depicts the total static and dynamic pressure acting on the runner blades. The total pressure is highest near the leading edge of the blade. Figure 10 shows velocity vectors passing through the computational domain in a stationary frame. Around the trailing

edge, the vectors depict a highly turbulent structure that has formed as expected. Figure 11 is a contour plot of velocity along the meridional and confirms the presence of a turbulent structure after the trailing edge of the blades. Finally, Figure 12 displays the wall shear stress acting on the runner due to the fluid flow. As the fluid approaches the trailing edge of the runner, the wall shear stress increases dramatically.

Figure 9: Total Pressure Contours at the Surface of the Blade

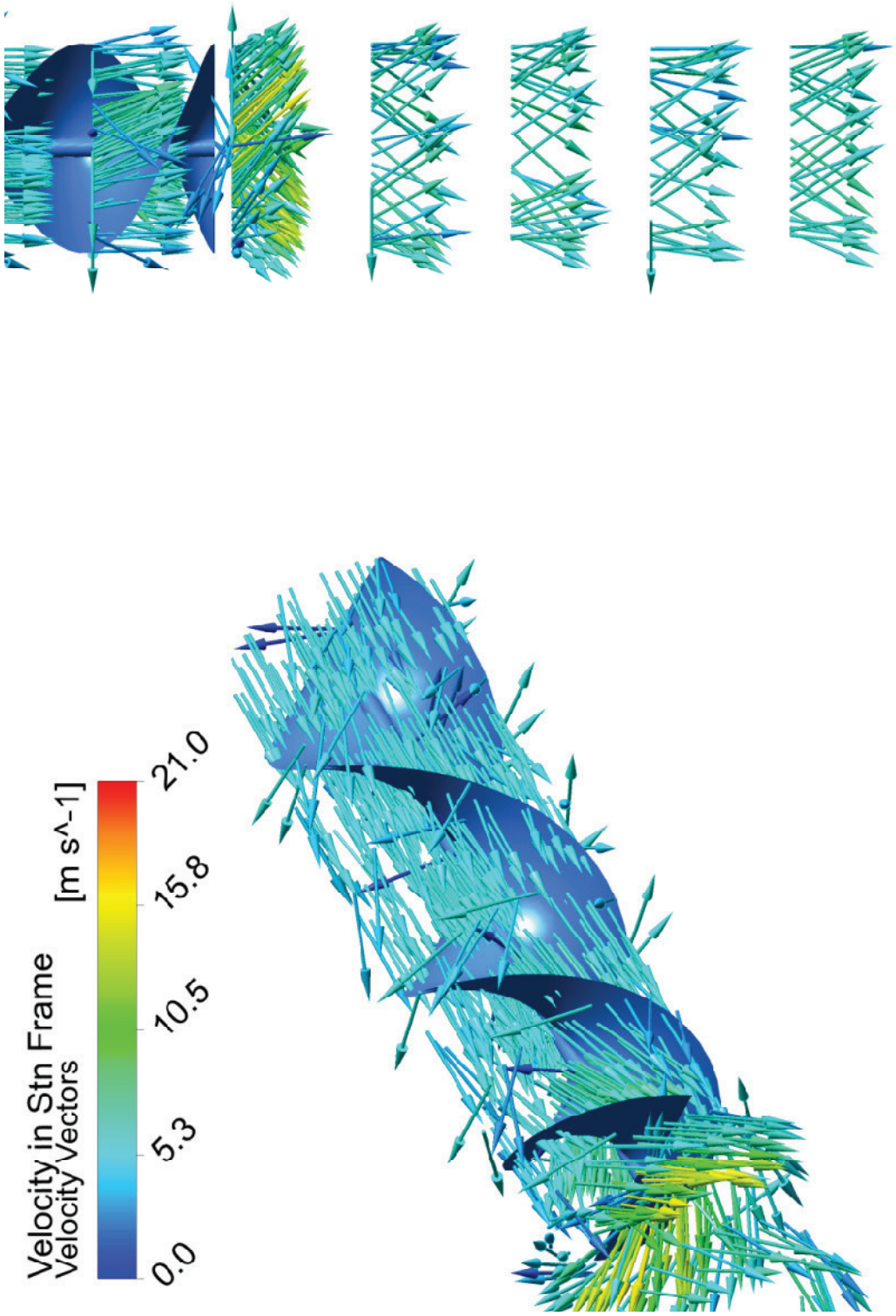

Figure 10: Velocity Vectors in the Stationary Frame

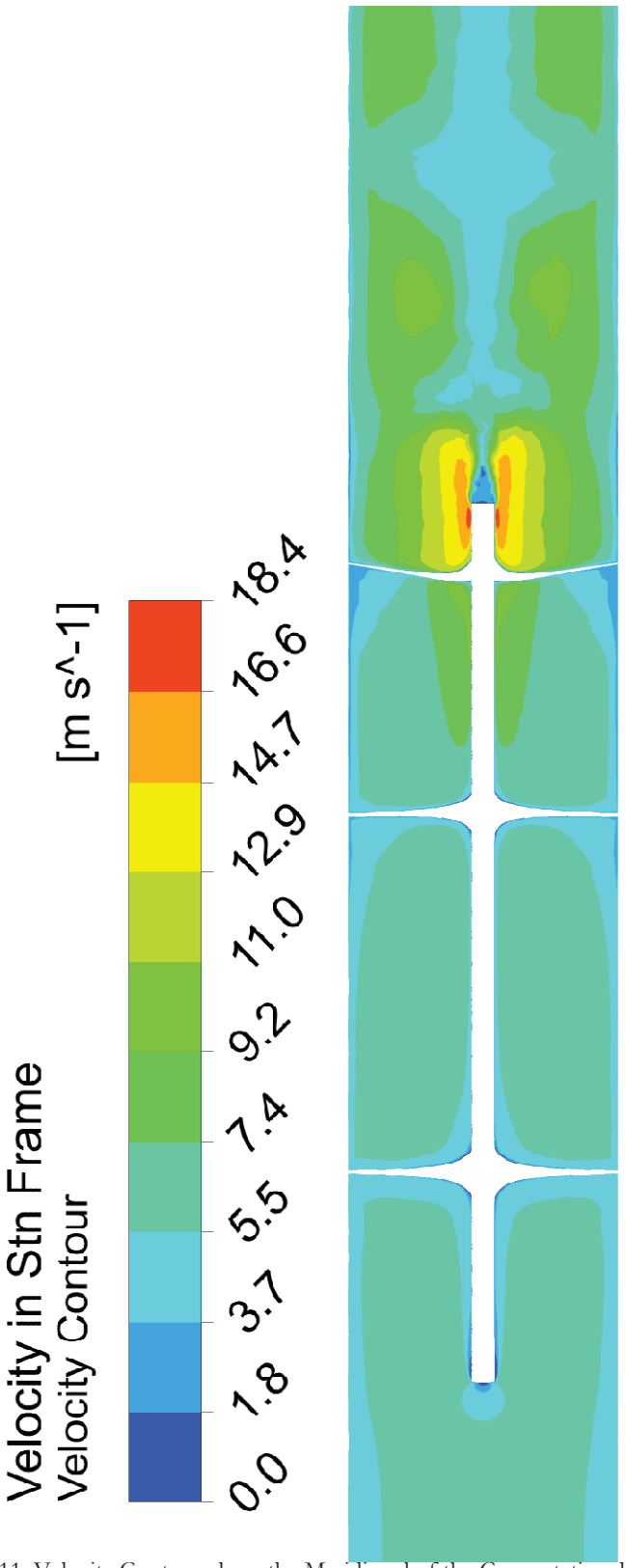

Figure 11: Velocity Contour along the Meridional of the Computational Domain

Figure 12: Contours of the Wall Shear Stress on the Surface of the Blade

THE ROTATING FRAME OF REFERENCE METHOD

The following figures are results for CFD simulations at 0.1 m^3/s and 750 RPM using the change of reference frame method. Figure 13 depicts the total static and dynamic pressure acting on the runner blades. The total pressure is highest near the leading edge of the blade. Figure 14 shows velocity vectors passing through the computational domain in a stationary frame. Around the trailing edge, the vectors depict a highly turbulent structure that has formed as expected. Figure 15 is a contour plot of velocity along the meridional and confirms the presence of a turbulent structure after the trailing edge of the blades. The vorticy rope that is present at the trailing edge of the runner as expected from the velocity vectors is illustrated in Figure 16. Figure 16 is an excellent illustration of the swirling flow structure created by the motion of the blades. The intensity of the vortex decreases away from the trailing edge of the blades. Finally, Figure 17 displays the wall shear stress acting on the runner due to the fluid flow. As the fluid approaches the trailing edge of the runner, the wall shear stress increases dramatically.

Figure 13: Total Pressure Contours at the surface of the Blade

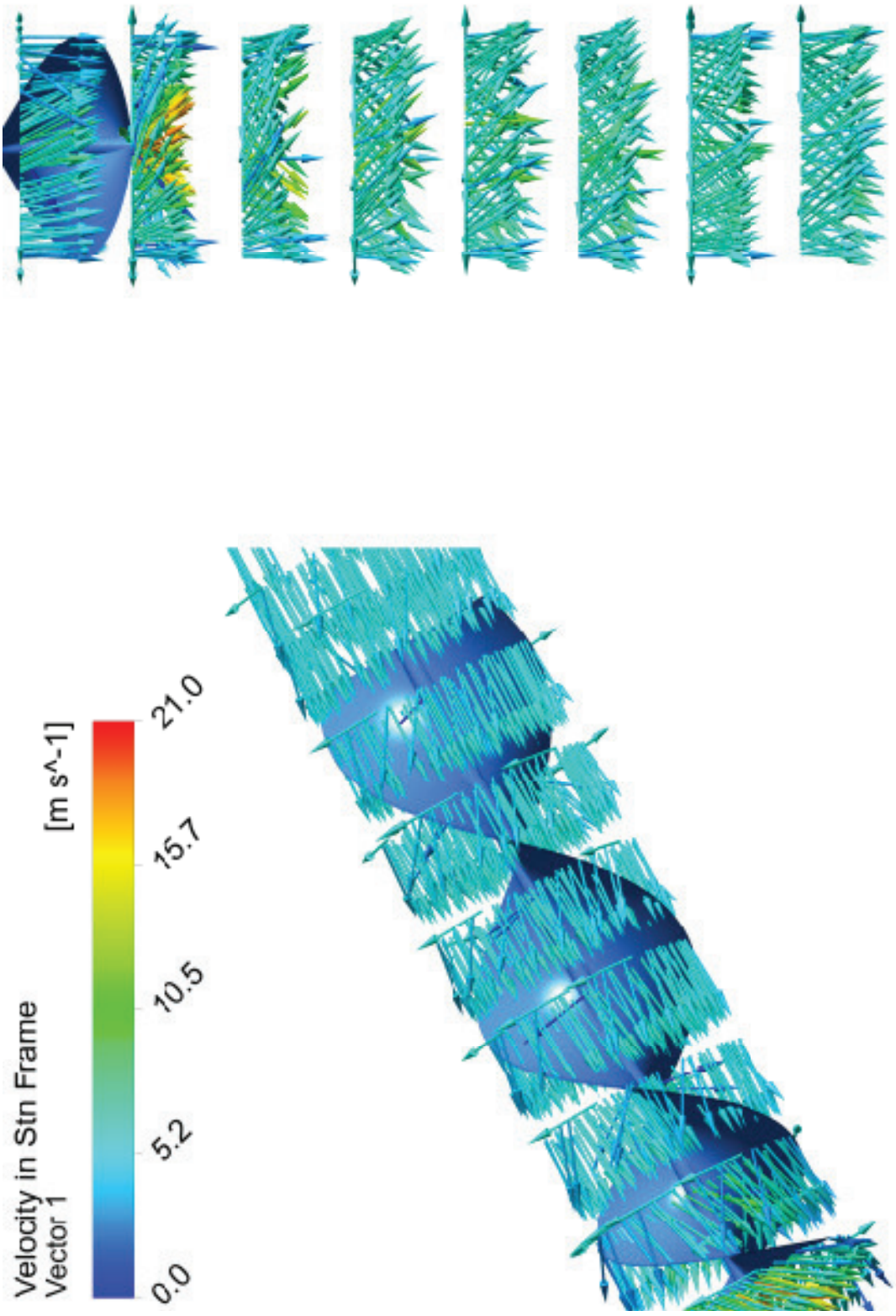

Figure 14: Velocity Vectors in the Stationary Frame

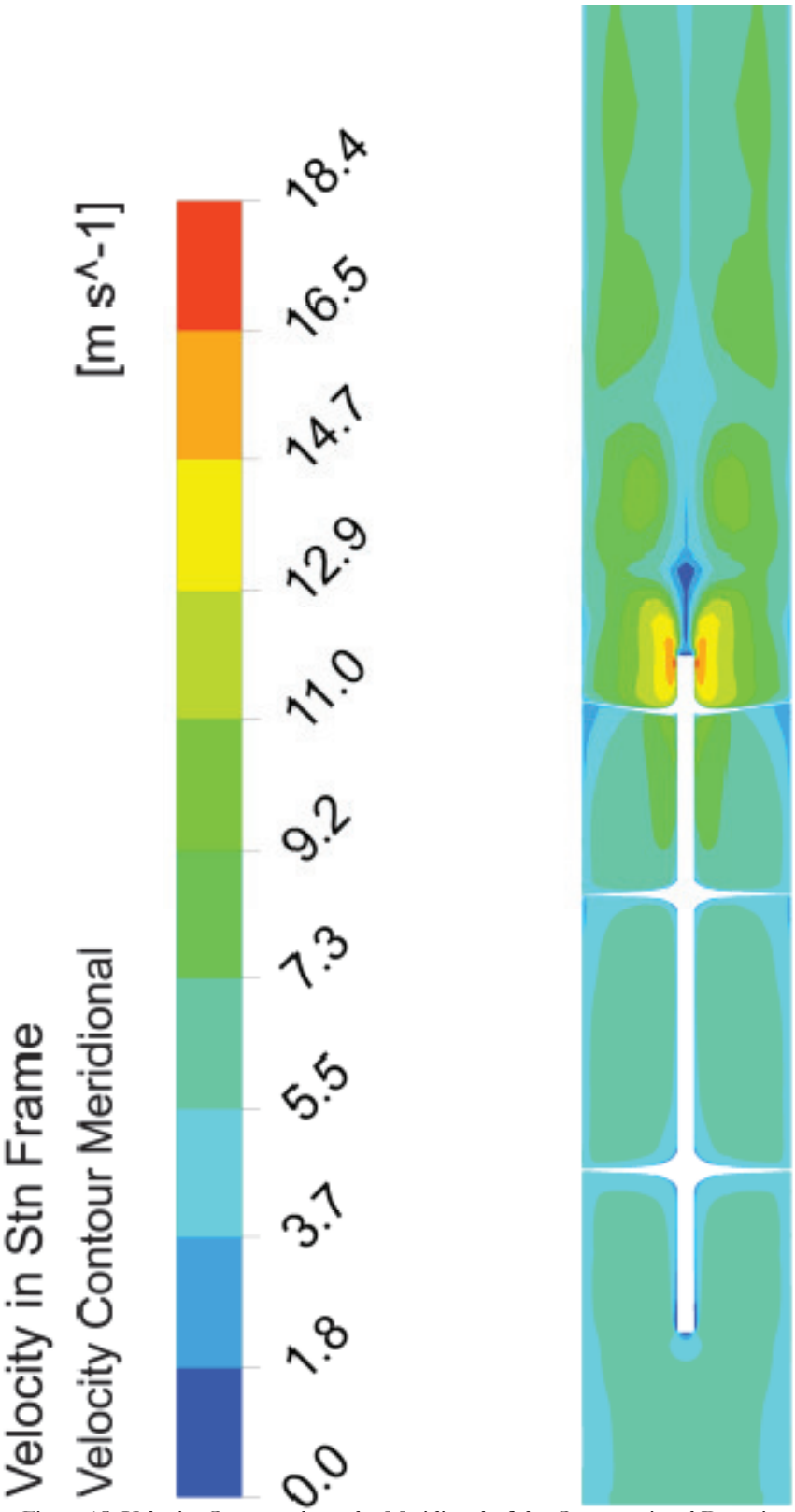

Figure 15: Velocity Contour along the Meridional of the Computational Domain

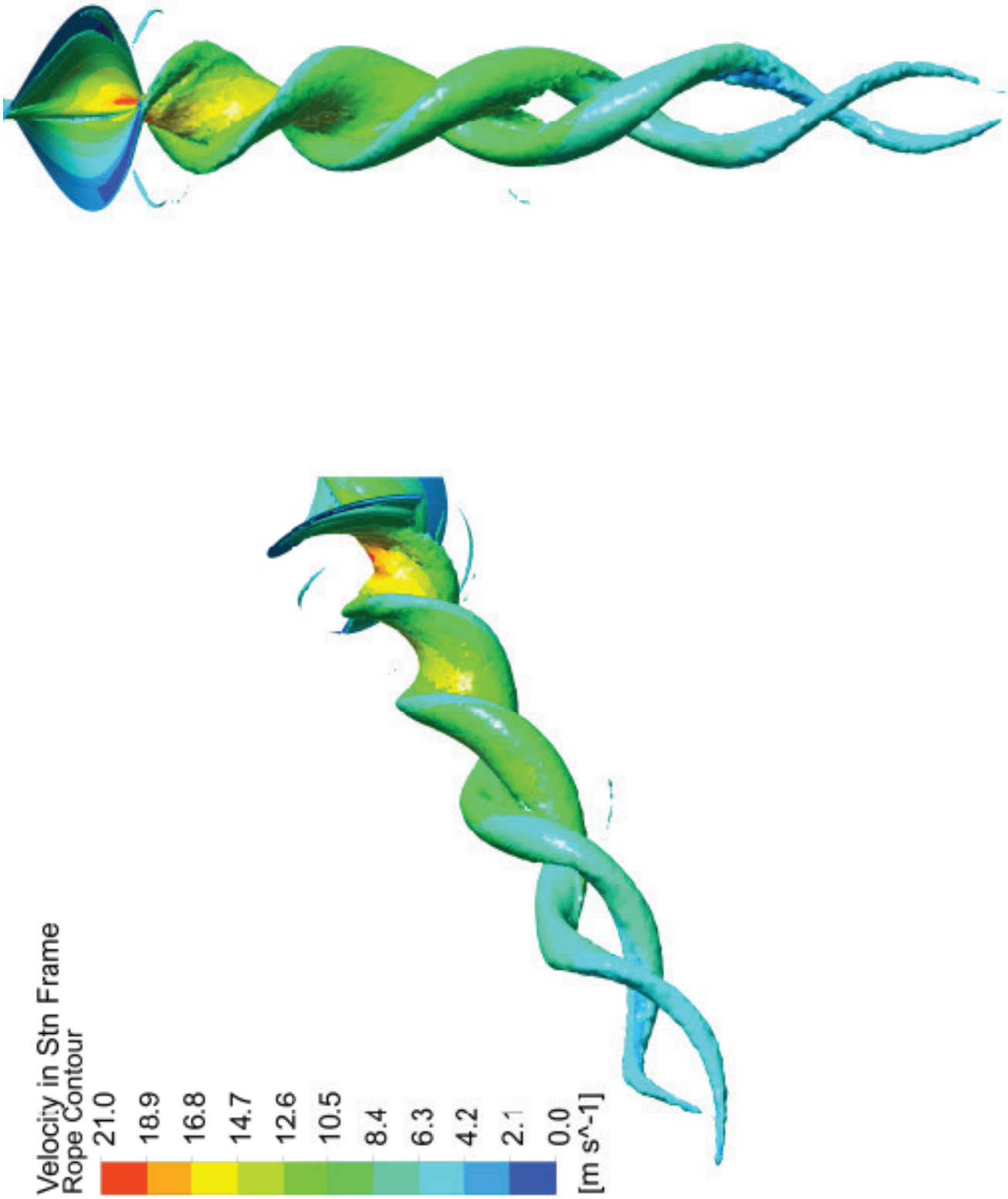

Figure 16: Vortex Rope with a Swirling Strength of 267.1 rad/s

Figure 17: Contours of the Wall Shear Stress on the Surface of the Blade

METHOD COMPARISON

Both the rotating mesh and the rotating frame of reference methods are two different means of producing similar results. Figure 9 and 13 are both total pressure contour plots on the blades for the same operating conditions, and are displayed with the same color scale. The results between the two figures are almost exactly the same, with some minute exceptions. The rotating mesh method shows that there is a slightly larger high pressure region at the outer edges of the blade on the leading edge than what was calculated with the frame of reference method. It also depicts a similar result from the low pressure region. These variances, however, could be due to the fact that a different mesh was used between the two calculations since the results were computed at different times during this study.

Figure 12 and 15 offer another comparison between the results of the two different methods. The notable differences between the two figures come in the solution starting near the trailing edge of the blade and heading downstream of the turbine. One noticeable difference is in the low velocity region downstream of the turbine. In the rotating mesh method, we see that the low velocity region is short, and forms the shape of a cone off of the shaft. In the frame of reference method, we see this low velocity region elongated further downstream of the turbine. Again, this could be due to the use of different meshes for the calculations. However, the reference frame method is known to smooth the transient effects of the solution which could also provide an explanation for the variation in results [16].

Differences between the calculated wall shear stress are also apparent between the two calculations as seen in Figure 12 and 17. The high area of wall shear stress appears to be more

predominate in the reference frame method than the rotating mesh method. Also, on the frame of reference method using the same color scale between the two results, there are little splotches of lower shear stress regions located on the outer radius of the blades in the middle area of the blades which are not apparent on the same plot for the rotating mesh method.

Moving to a macroscopic view of the results, the performance results are similar between calculations as well. The definition of these performance parameters will be explained later in this paper. The power calculated by the rotating mesh method has been determined to be 2248 Watts, as to be compared with the reference frame method which was determined to be 2359 Watts. The percent difference between these two results is about 5%. The calculated head required for each of these simulations is 3.232 meters for the rotating mesh and 3.224 meters for the reference frame method, differing by about 0.2%. Finally, the calculated efficiency for the rotating mesh is 72% as compared to the reference frame's efficiency of 74% for a difference of about 3%. These performance results indicate that the solutions between these two methods are similar. The reference frame method appears to have a higher prediction in performance characteristics. It can be due to the mentioned smoothing of the transient nature of the solution, which is known to over predict turbulence parameters in k-epsilon models such as the model used between these two simulations. Without any physical test data such as Laser Doppler Velocimetry (LDV) measurements, this claim can be hard to make [17] [18] [19].

THE EFFECT OF FLOW RATE ON THE FLOW REGIME

The effect of volumetric flow rate has a strong influence on the performance of the turbine and in the flow regime. The following figures represent the solution using the rotating mesh method, with a constant rotation rate of 750 RPM. The flow rates chosen for these comparisons are 0.05 m^3/s, 0.1 m^3/s and 0.2 m^3/s.

Figures 9 (Page 28), 18 and 19 are comparisons of the total pressure contours at the surface of the blade for each of the prescribed flow rates using the same color scale. Figure 18 is the result for the lower flow rate (0.05 m^3/s) and shows a pretty even distribution in the total pressure acting on the blade. As flow rate increase to Figure 9 (0.1 m^3/s), it is seen that the uniform total pressure distribution has increased, and a much higher pressure gradient is seen in the trailing edge region. This trend is exaggerated even more as the flow rate increases to 0.2 m^3/s in Figure 19 where the gradient is even more apparent.

Figures 10 (Page 29), 20 and 21 show insight into the velocity vectors at various planes in the computational domain. As expected, the trend shows that velocity increases as flow rate increases. However, as the flow rate increases the gradient in the velocity field at the trailing edge and downstream is much greater. The turbulent nature of the flow becomes more apparent as the flow rate increases.

Figures 11 (Page 30), 22 and 23 depict a velocity contour along the meridional of the computational domain. As flow rate increases the velocity near the trailing edge greatly increases, and the effect of this increase travels up the blade. Downstream of the turbine, it is seen that an area of low pressure forms in the center of the domain and depicts the swirling

nature of the flow after the trailing edge. This can be confirmed with Figure 16 which shows a model of this swirling structure.

Finally Figures 12 (Page 31), 24 and 25 compare the calculated wall shear stress by the fluid. As expected as the flow rate increases, the wall shear stress increases. It greatly increases in the trailing edge region especially around the blade-to-shaft interface. Both the wall shear stress and total pressure contours at the higher flow rates suggest that the onset of cavitation may be apparent on these surfaces. A thesis by a fellow student in this research group by Jacob Riglin discusses this issue of cavitation in more detail [20].

Figure 18: Total Pressure Contour at the Surface of the Blade - Flow Rate 0.05 CMS

Figure 19: Total Pressure Contours at the Surface of the Blade - Flow Rate 0.2 CMS

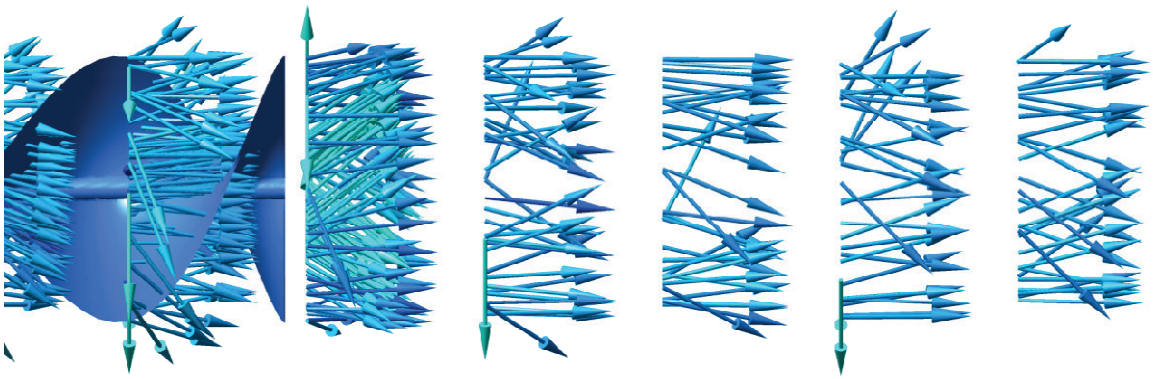

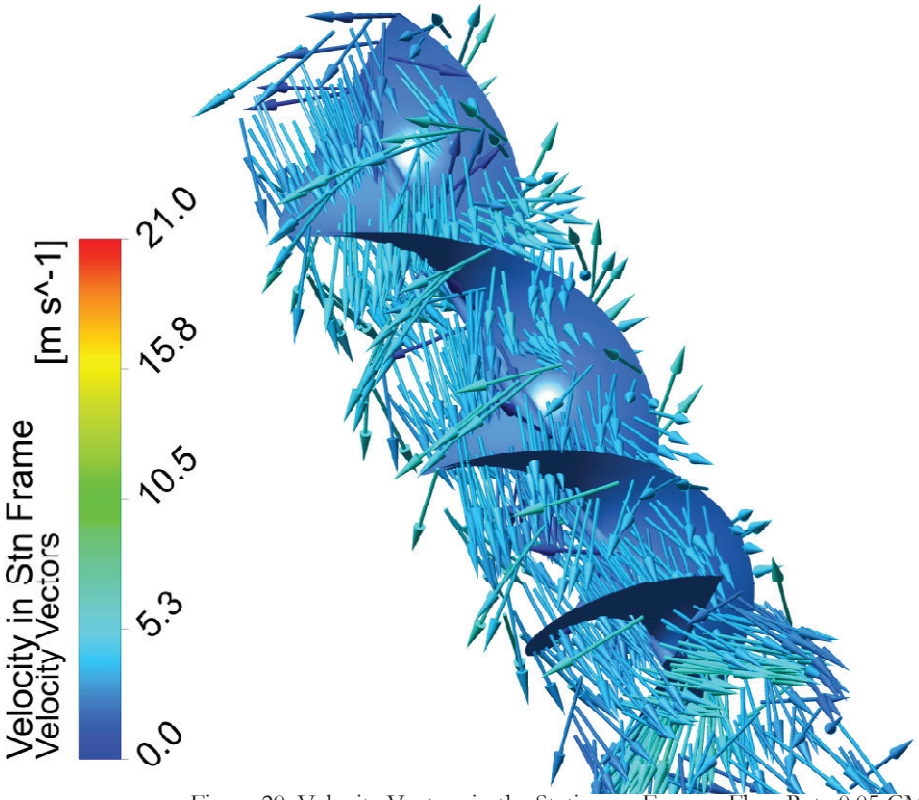

Figure 20: Velocity Vectors in the Stationary Frame - Flow Rate 0.05 CMS

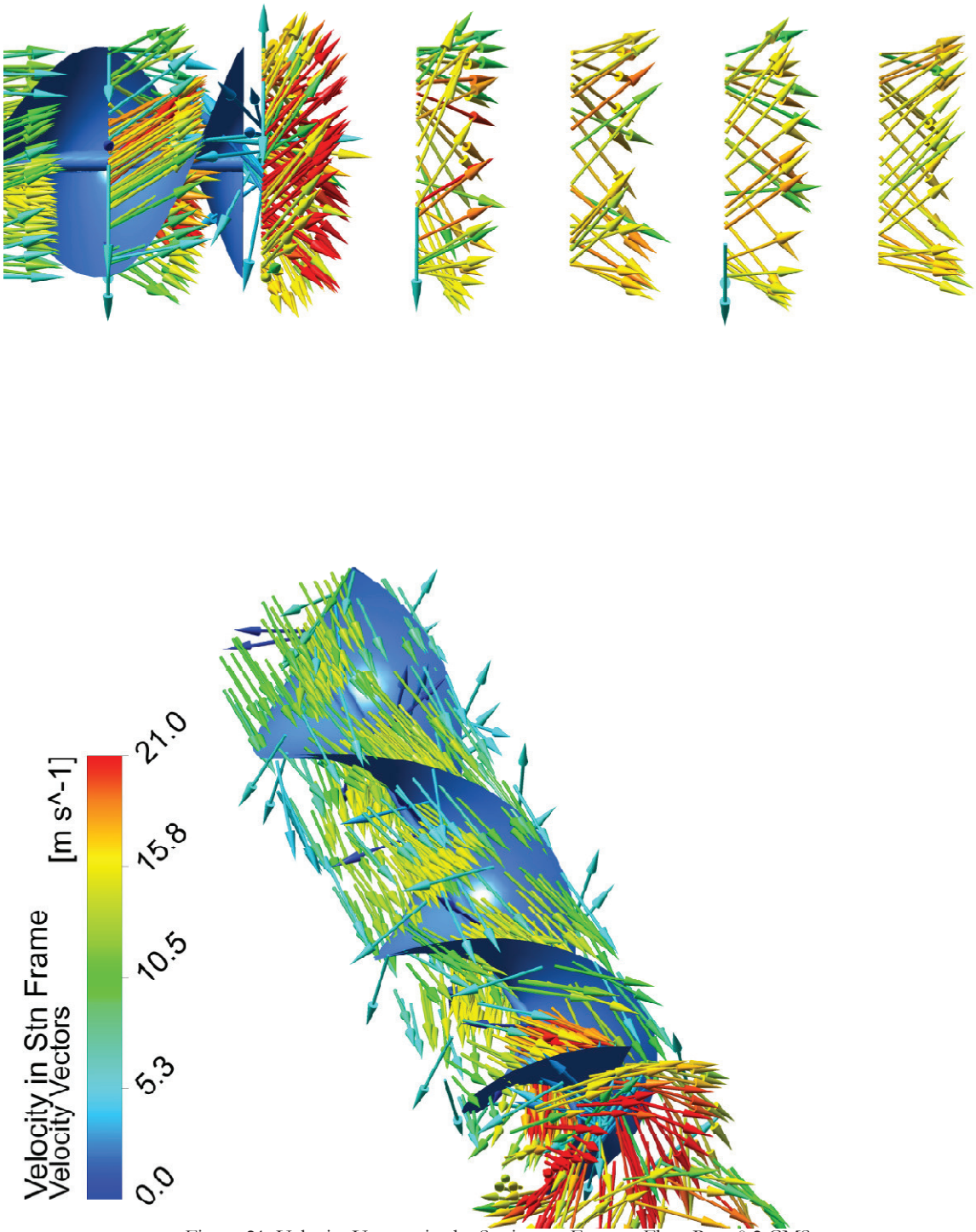

Figure 21: Velocity Vectors in the Stationary Frame - Flow Rate 0.2 CMS

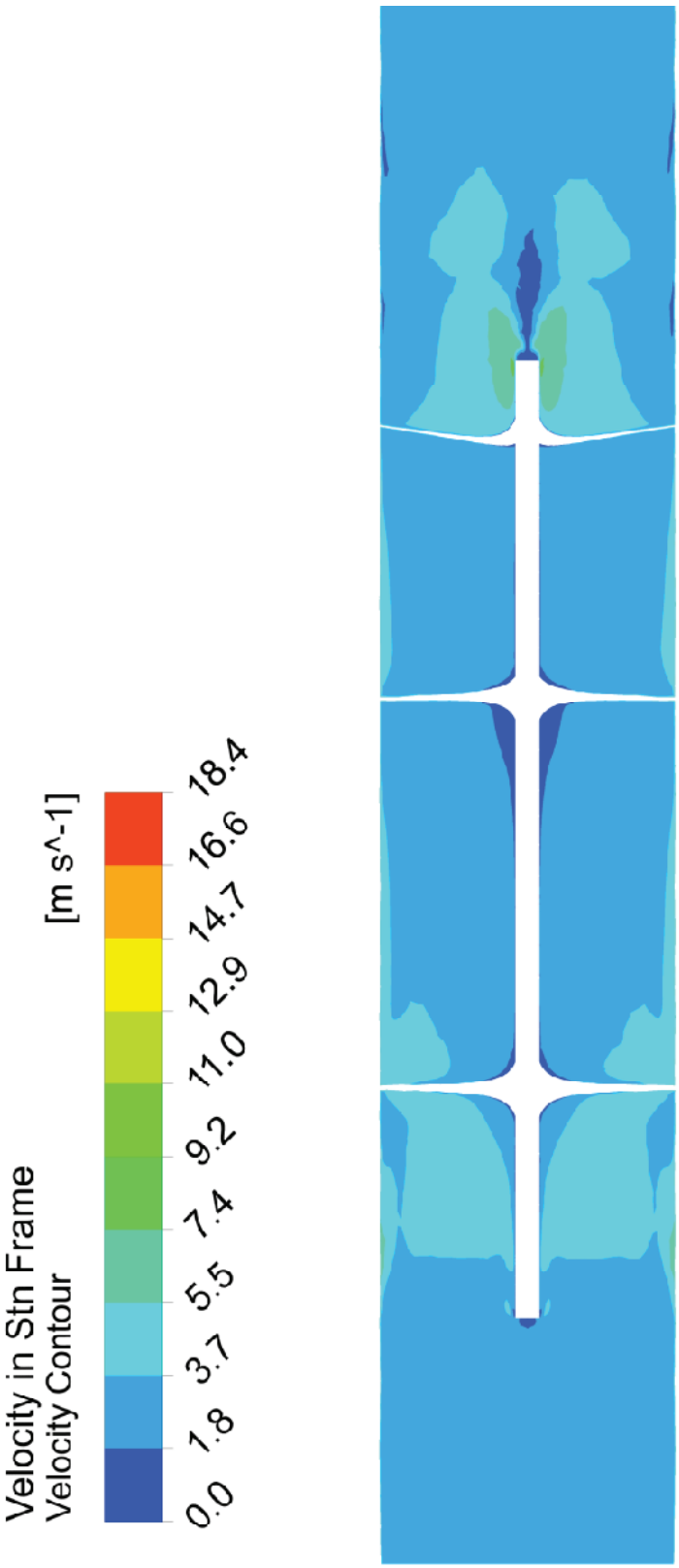

Figure 22: Velocity Contour along the Meridional of the Computational Domain - Flow Rate 0.05 CMS

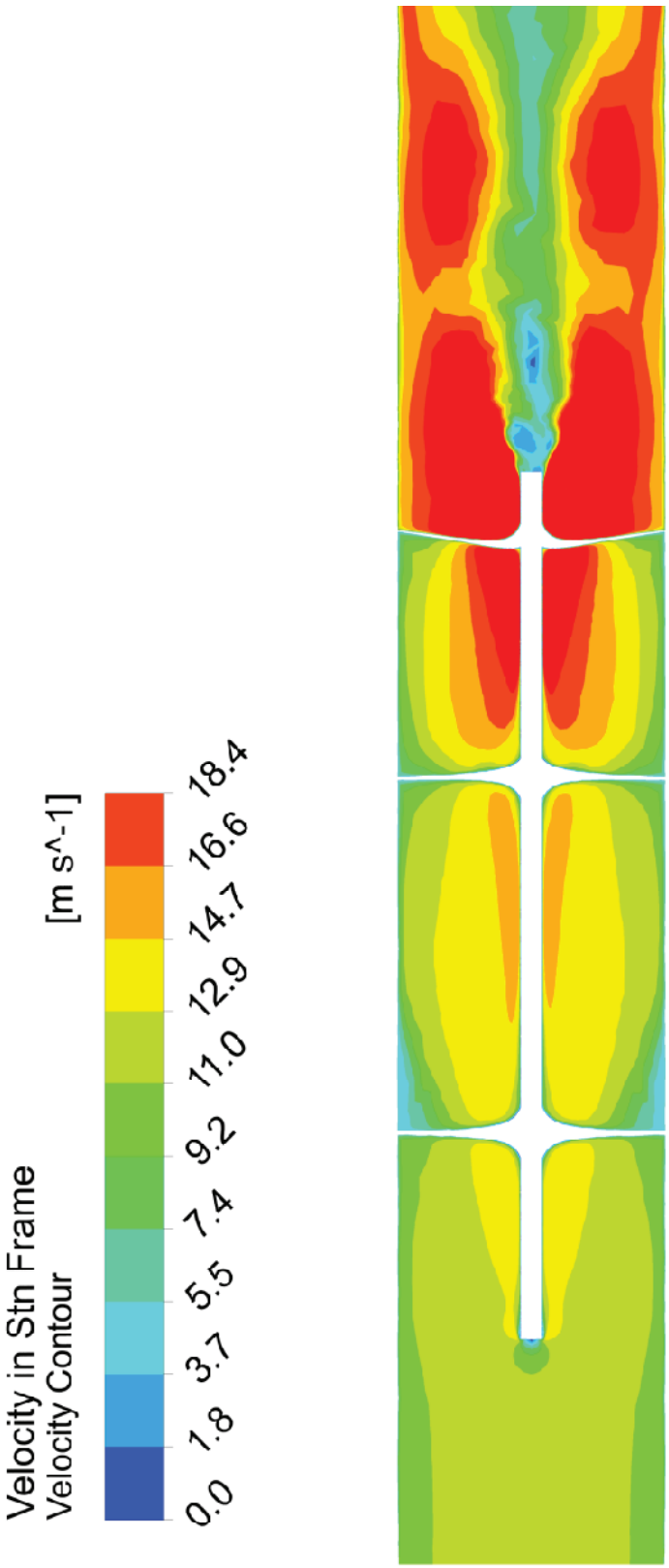

Figure 23: Velocity Contour along the Meridional of the Computational Domain - Flow Rate 0.2 CMS

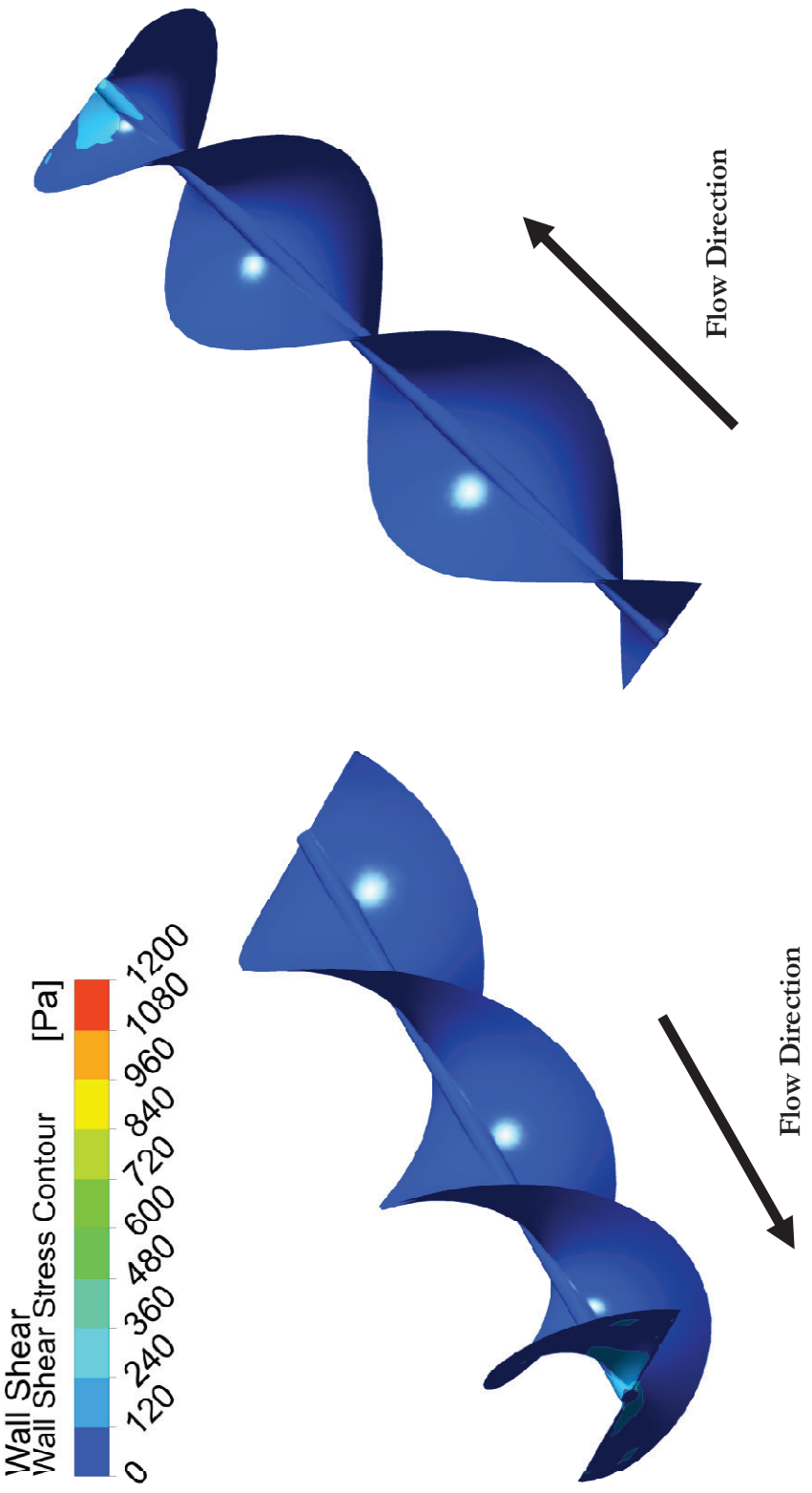

Figure 24: Contours of the Wall Shear Stress on the Surface of the Blade - Flow Rate 0.05 CMS

Figure 25: Contours of the Wall Shear Stress on the Surface of the Blade – Flow Rate 0.2 CMS

THE EFFECT OF ROTATION RATE ON THE FLOW REGIME

The effect of rotation rate has an influence on the performance of the turbine and in the flow regime, but not as strong as flow rate. The following figures represent the solution using the rotating mesh method, with a constant flow rate of 0.1 m^3/s. The rotation rates chosen for these comparisons are 250 RPM, 500 RPM, and 750 RPM.

Figures 9 (Page 28), 26 and 27 are comparisons of the total pressure contours at the surface of the blade for each of the prescribed rotation rates using the same color scale. All three figures show a very similar solution in the total pressure distribution. The only slightly noticible difference is the low total pressure region at the trailing edge of the blade varries slightly. Rotation rate appears to have only a slight effect on this distributuion.

Figures 10 (Page 29), 28 and 29 show insight into the velocity vectors at various planes in the computational domain. No noticible difference between these vectors for each rotation rate can be seen. This again shows that the rotation rate of the blade has little effect on the solution.

Figures 11 (Page 30), 30 and 31 depict a velocity contour along the meridional of the computational domain. The solutions are again very similar, however the contours show some noticible differences in the solution. The high velocity region at the trailing edge of the blade is larger at the slower rotation rates and decreases in size as rotation rate increases.The low velocity region downstream of the turbine is also larger for the slower rotation rates and decreases as rotation rate increases.

Finally Figures 12 (Page 31), 32 and 33 compare the calculated wall shear stress by the fluid. Difference between solutions can been seen in these figures.At the slower rotation rate, the wall shear stress is greater closer to the leading edge and middle section of the blade than the other two greater rotation rates. The trend appears to be that as rotation rate increases, shear stress becomes more concentrated in the trailing endge section. The max shear stress area also seems to be larger in the fastest rotation rate than in the slower rotation rates.

Figure 26: Total Pressure Contour at the Surface of the Blade - Rotation Rate 250 RPM

Figure 27: Total Pressure Contour at the Surface of the Blade - Rotation Rate 500 RPM

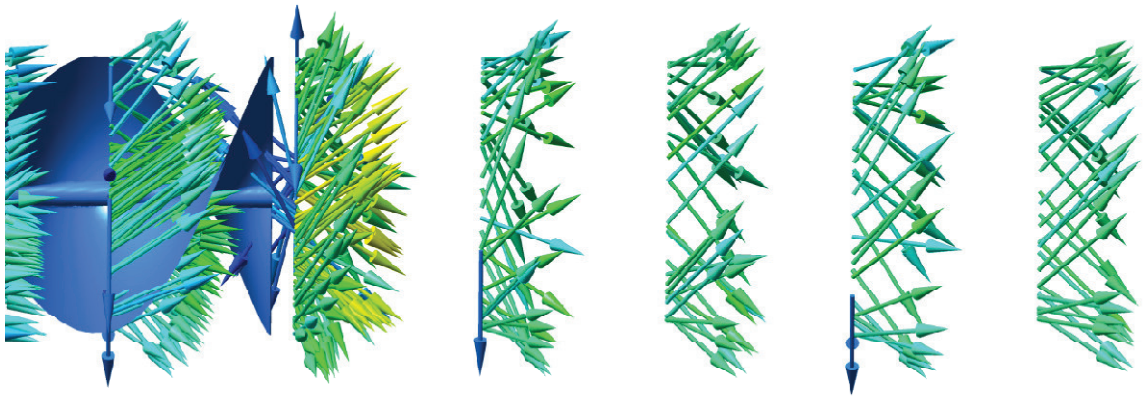

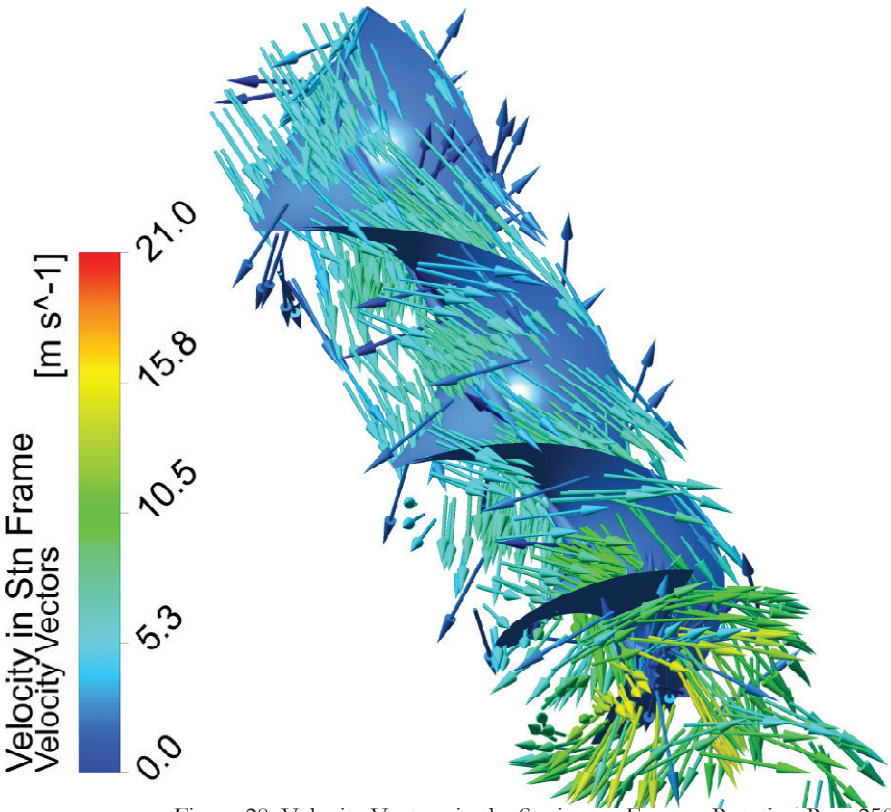

Figure 28: Velocity Vectors in the Stationary Frame - Rotation Rate 250 RPM

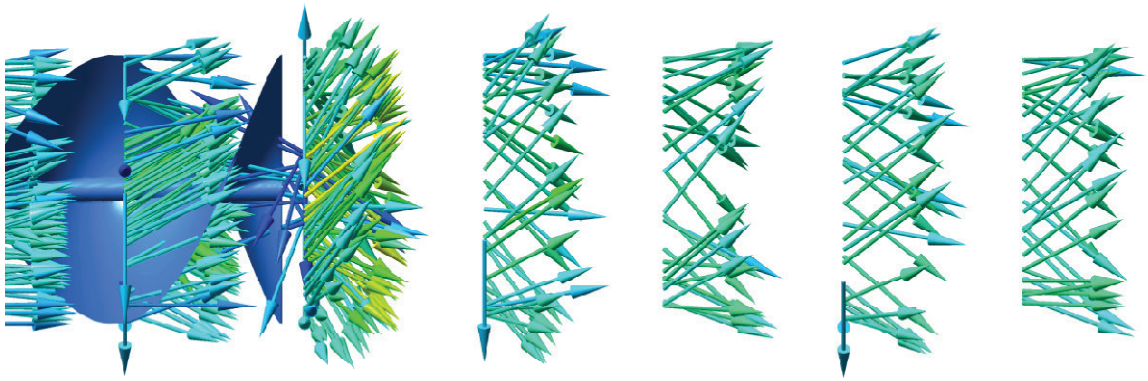

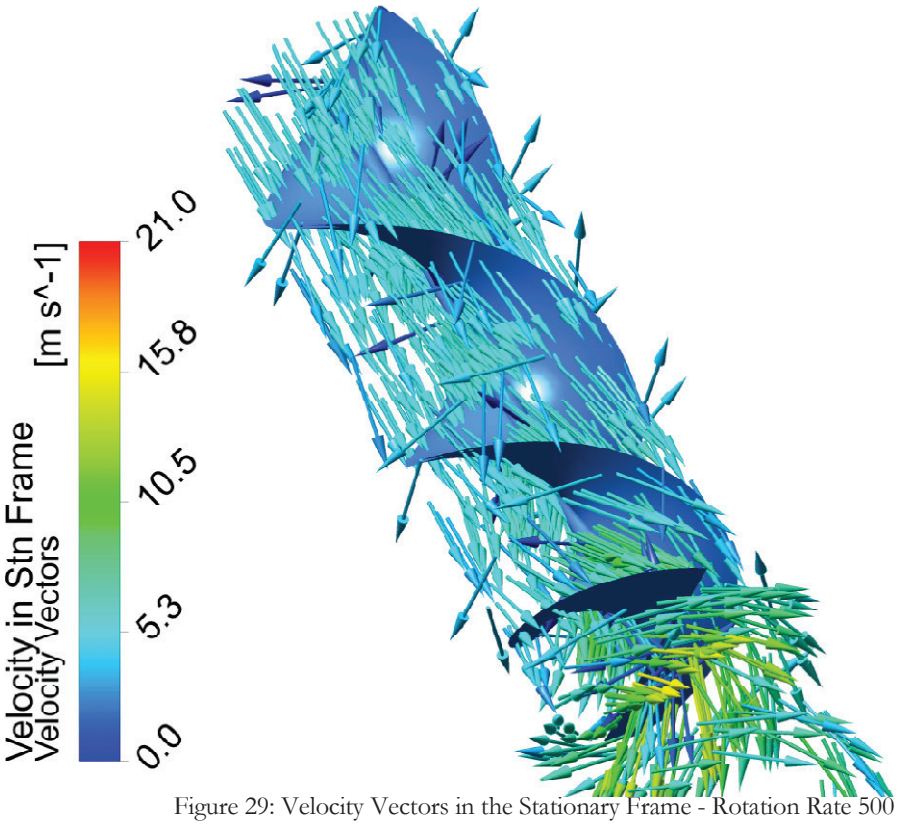

Figure 29: Velocity Vectors in the Stationary Frame - Rotation Rate 500 RPM

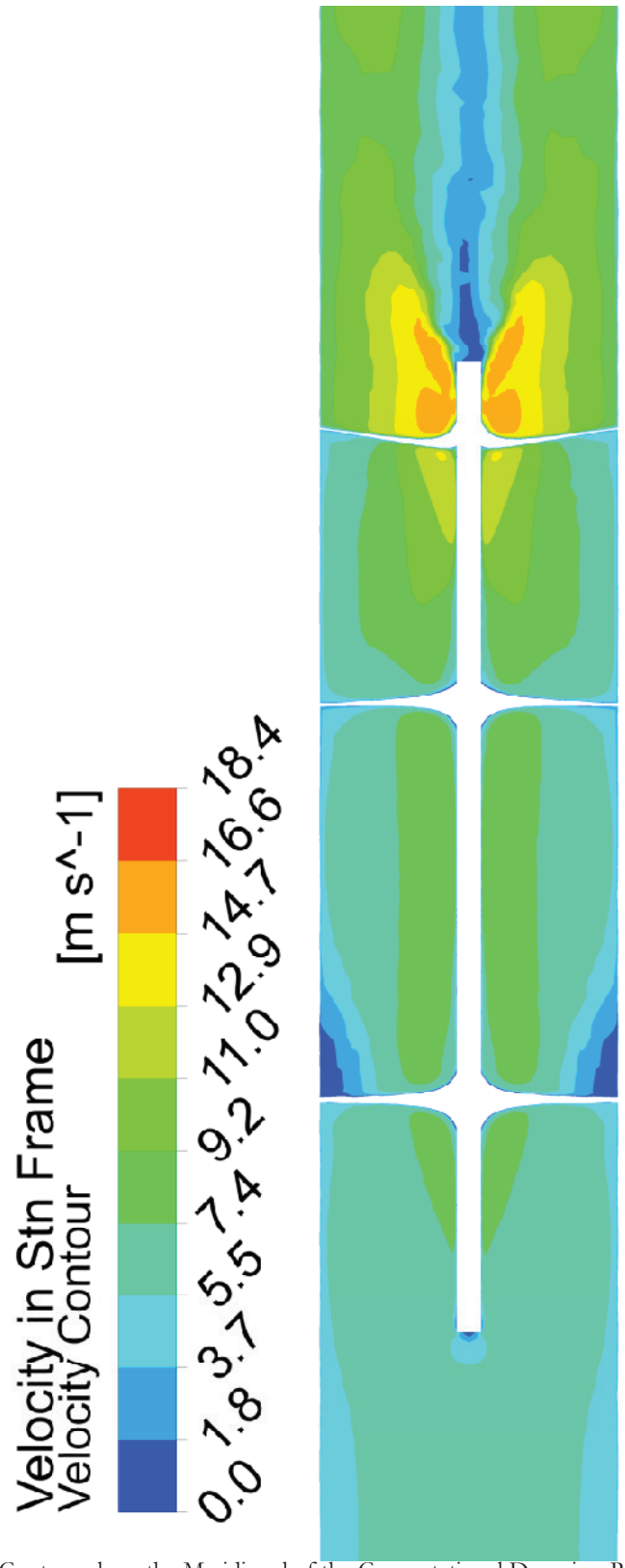

Figure 30: Velocity Contour along the Meridional of the Computational Domain - Rotation Rate 250 RPM

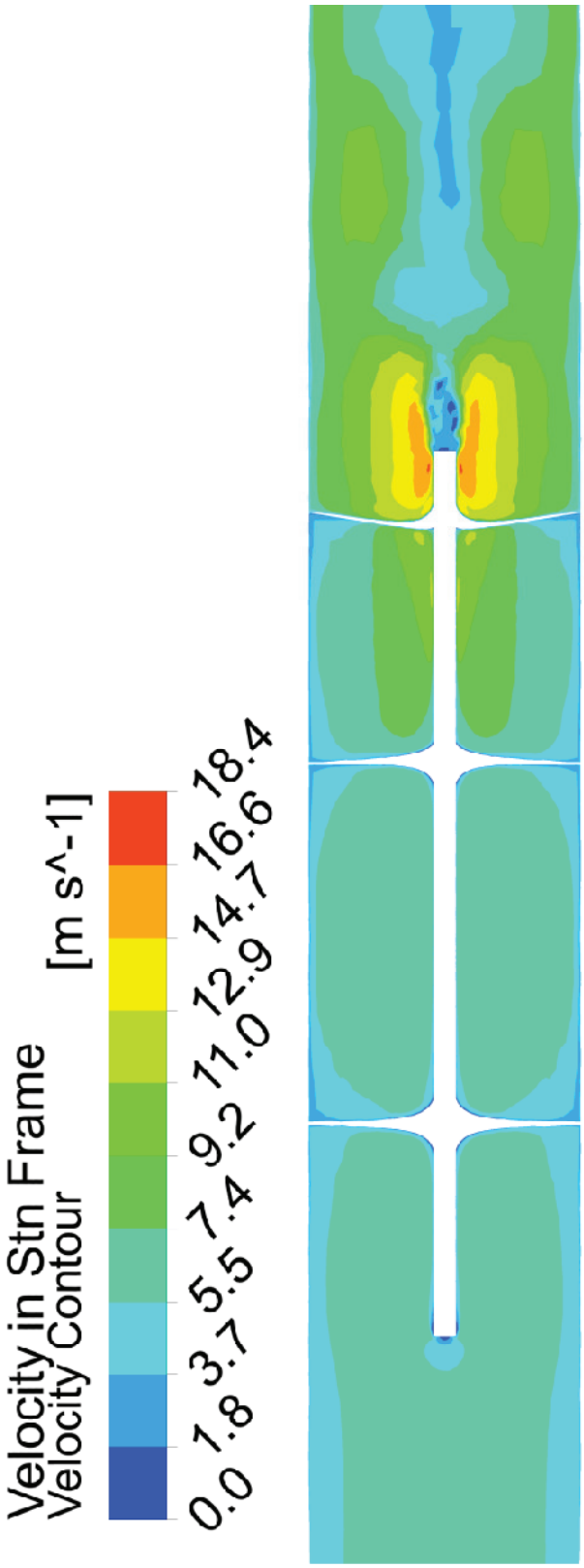

Figure 31: Velocity Contour along the Meridional of the Computational Domain - Rotation Rate 500 RPM

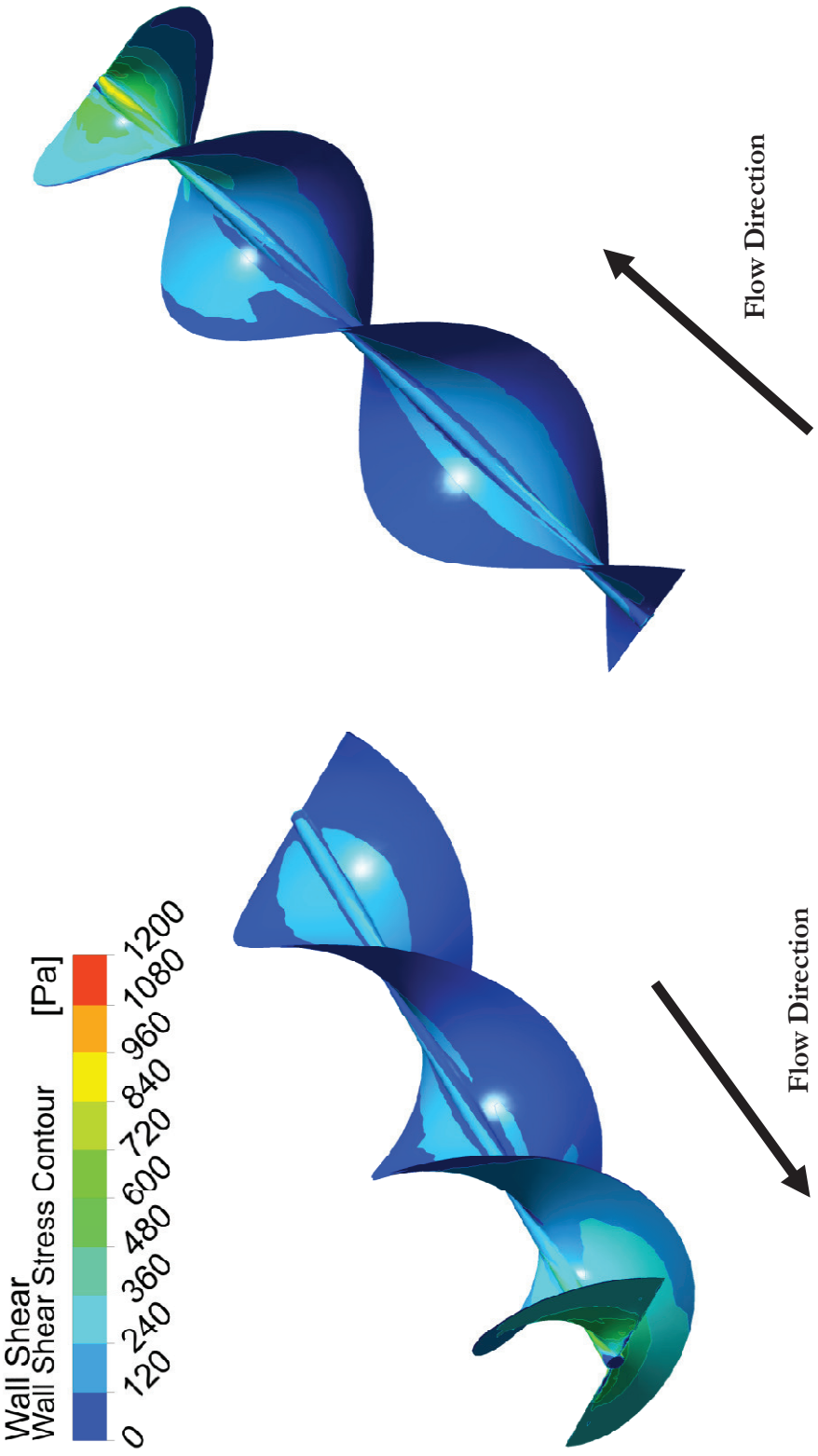

Figure 32: Contours of the Wall Shear Stress on the Surface of the Blade - Rotation Rate 250 RPM

Figure 33: Contours of the Wall Shear Stress on the Surface of the Blade - Rotation Rate 500 RPM

UNIFORM VERSUS NON-UNIFORM PITCH

This thesis has stressed the importance of non-uniform pitch in these Archimedean screw designs. The following results are a comparison with a uniformly pitched screw and show why this non-uniform pitch is an important aspect to the design. The results shown are for a flow rate of 0.1 m^3/s and rotation rate of 750 RPM.

Figures 9 (Page 28) and 34 depict the total pressure acting on the blade. The uniformly pitched blade does not have has much of a total pressure change between the leading and trailing edges of the blade as seen in the non-uniformly pitched blade. Also the total pressure extremes are much higher for the non-uniform pitch than the uniform pitch.

Figures 10 (Page 29) and 35 compare the velocity vectors at various planes in the computational domain. For the non-uniform case, the velocity vectors indicate a high amount of swirl downstream of the turbine, and a fast flow near the trailing edge of the blade. In the uniform case, the swirl is significantly not as strong as the non-uniform case. The velocities themselves are not varying much either as is seen in the non-uniform case. These two observations are also evident in comparing the velocity contours of Figure 11 (Page 30) and Figure 36.

Finally, the difference between the wall shear stress between Figures 12 (Page 31) and 37 is clearly evident. The wall shear stress in the uniform case is pretty low throughout the entire blade, while in the non-uniform case, the wall shear stress greatly increases toward the trailing edge of the blade.

Figure 34: Total Pressure Contours at the Surface of the Blade - Uniform Pitch

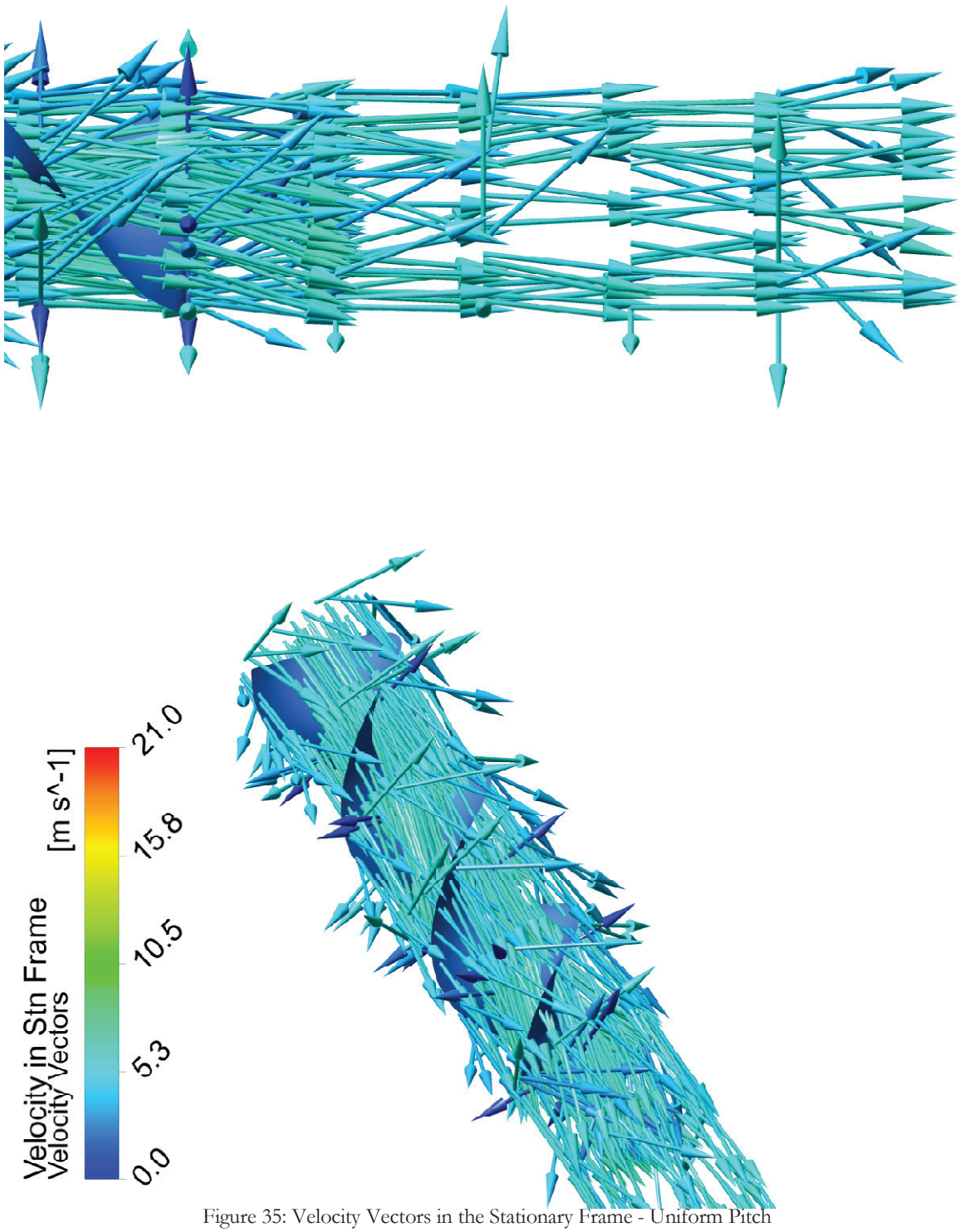

Figure 35: Velocity Vectors in the Stationary Frame - Uniform Pitch

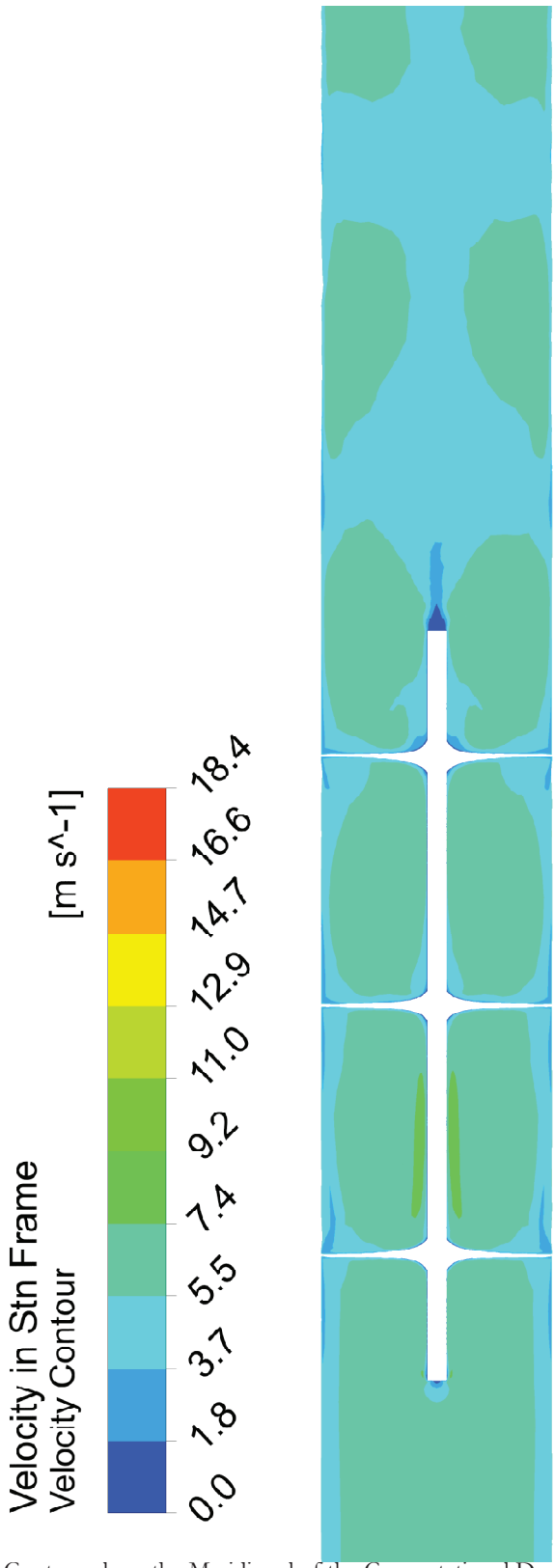

Figure 36: Velocity Contour along the Meridional of the Computational Domain - Uniform Pitch

Figure 37: Contours of the Wall Shear Stress on the Surface of the Blade - Uniform Pitch

MAPPING OF PERFORMANCE CHARACTERISTICS

In this investigation, the trend in required head, total power, and efficiency are calculated over a range of volumetric flow rates and rotation rates. The investigation was concerned with volumetric flow rates ranging from 0.05 m^3/s to 0.5 m^3/s and with rotation rates ranging from 200 RPM to 1500 RPM. The results were calculated from the transient simulation solutions. The total dynamic and static pressure was measured at a region just before and after the leading and trailing edges of the blades, respectively. The following equations were used to determine these performance characteristics.

$$Calculated\ Head = \Delta H_{turb.} = \frac{\Delta P_{Stat.+Dynam.}}{\rho_w g} \quad \textbf{(15)}$$

$$Calcualted\ Power = P_{turb.} = \tau_{blade}\Omega_{blade} \quad \textbf{(16)}$$

$$Calculated\ Efficiency = \eta_{turb.} = \frac{P_{turb.}}{\rho_w g \Delta H_{turb.} Q} \times 100\% \quad \textbf{(17)}$$

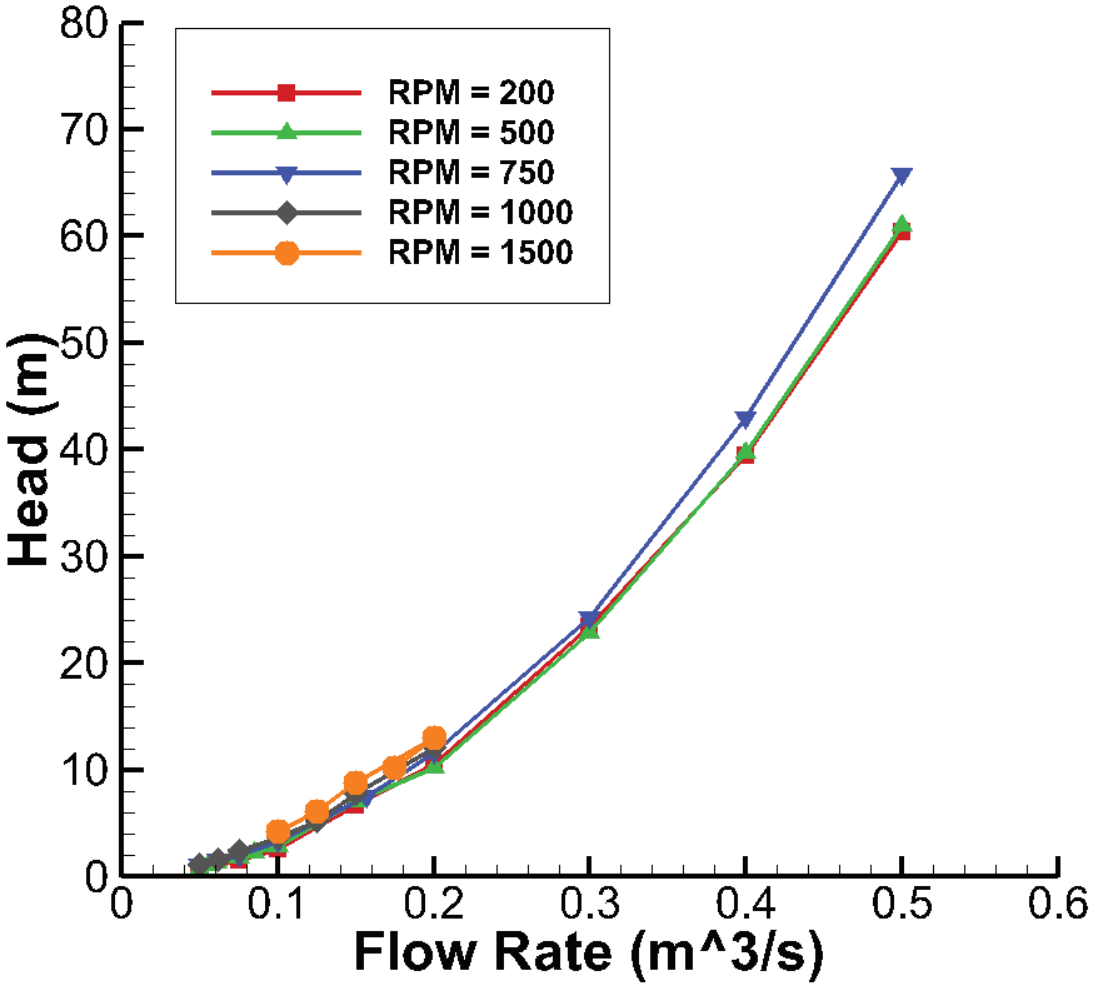

Figure 38: Calculated Head as a Function of Flow Rate for various Rotation Rates

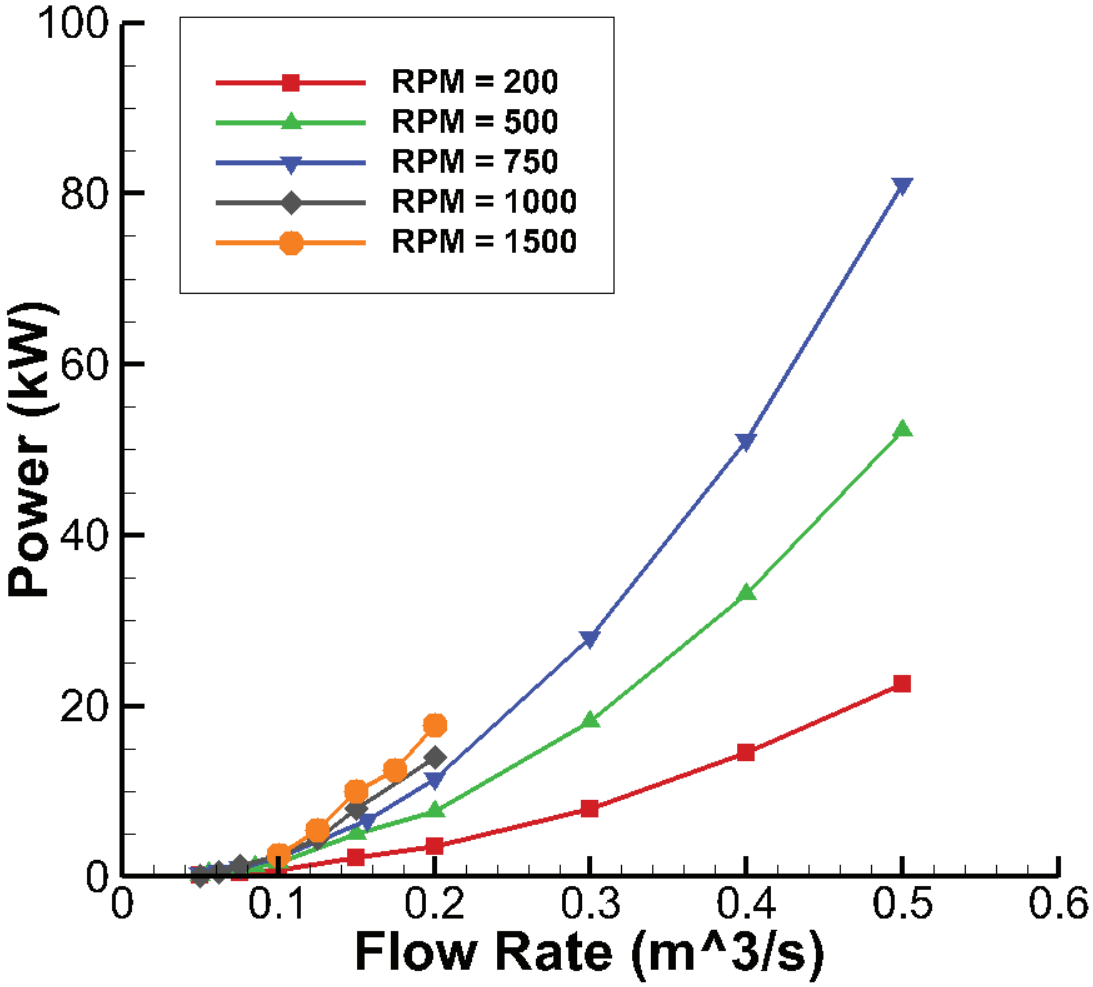

Figure 39: Calculated Power as a Function of Flow Rate for various Rotation Rates

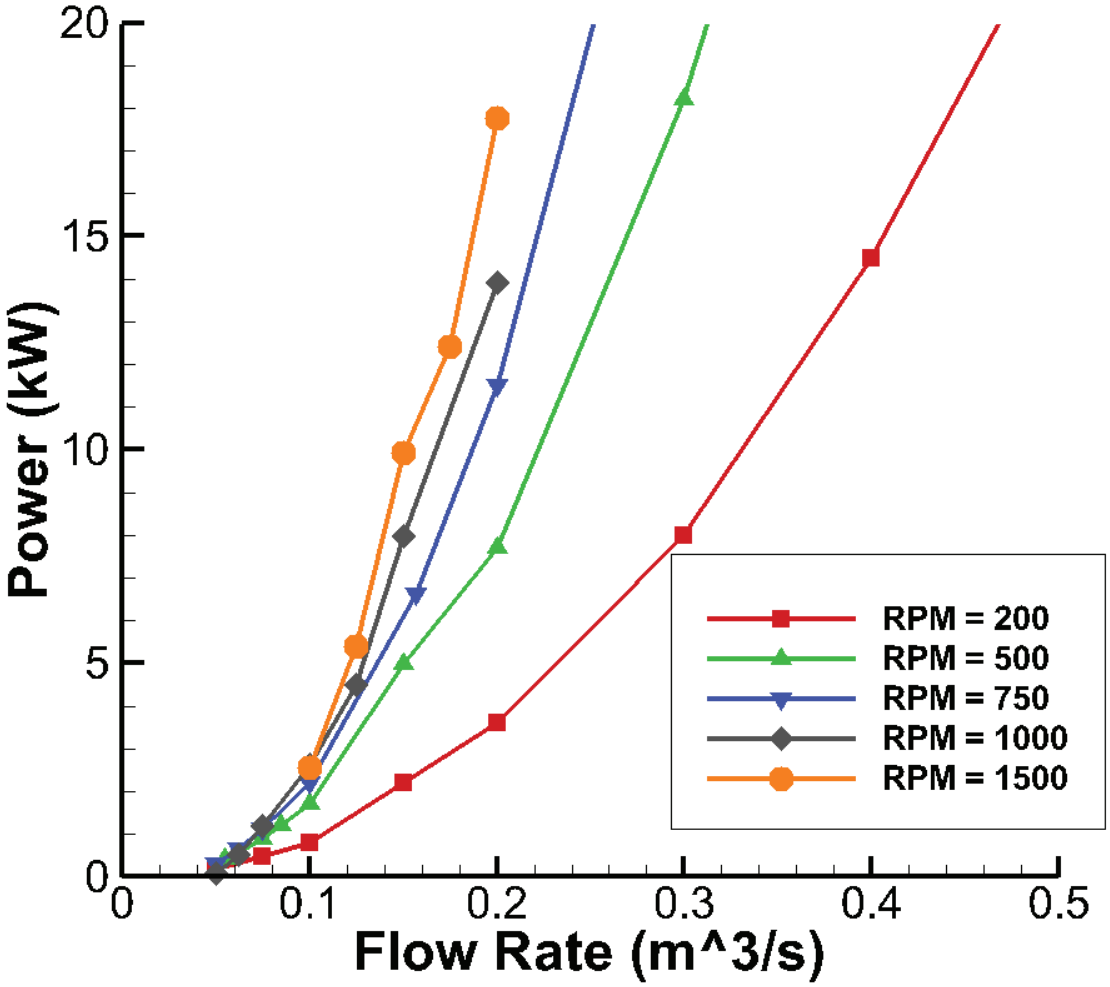

Figure 40: Calculated Power (closer look) as a Function of Flow Rate for various Rotation Rates

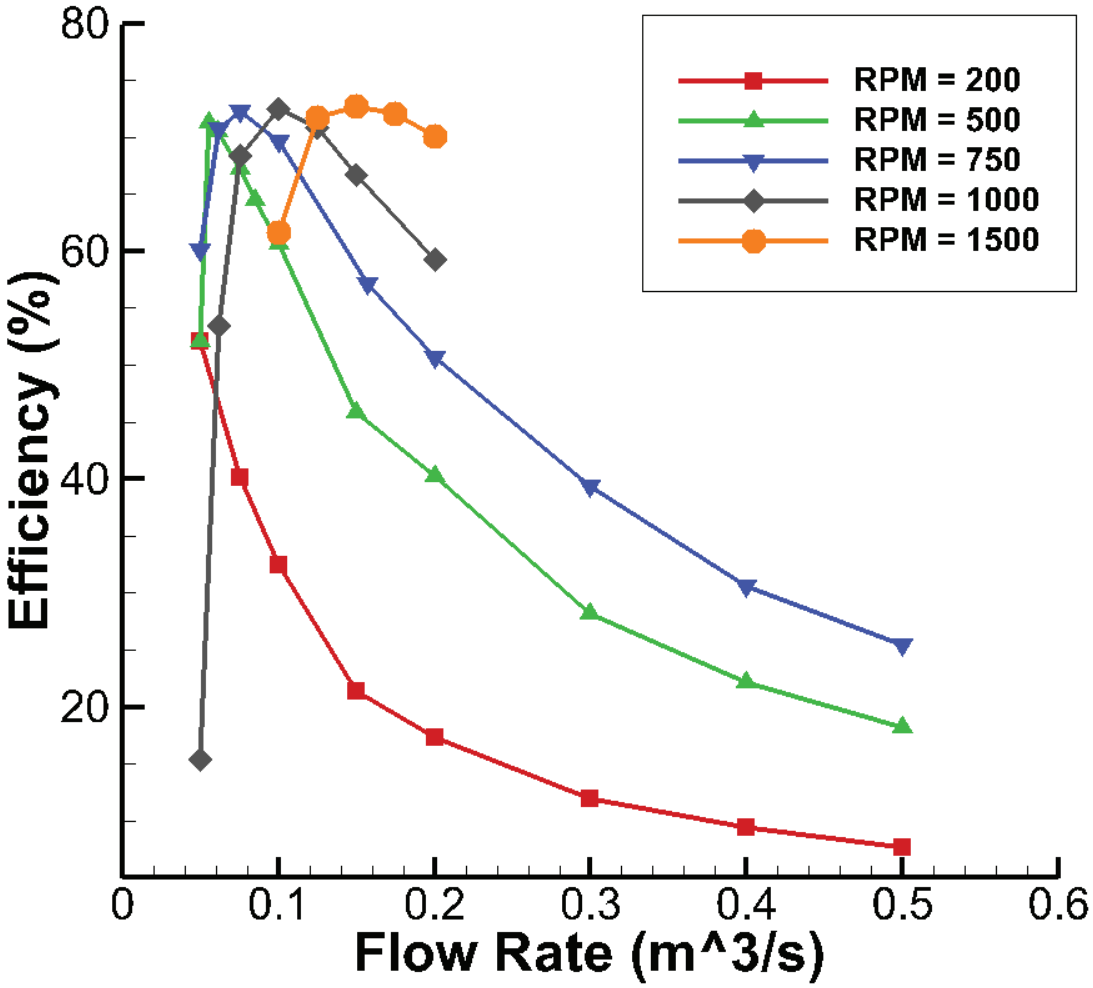

Figure 41: Calculated Efficiency as a Function of Flow Rate for various Rotation Rates

Calculated head, power and efficiency are plotted as a function of flow rate in Figure 38 through 41. Figure 38 shows the trend of the calculated required head versus the inlet volumetric flow rate over a range of rotation rates. The trend shows that no matter the rotation rate, the required calculated head for that flow rate is approximately the same. It only starts to vary more around the higher volumetric flow rates (approximately 0.4 m^3/s). Figure 39 and 40 display the trend in calculated power versus volumetric flow rate over a range of rotation rates. Here, it is seen that power increases exponentially as the calculated head does. However, rotation rate has a drastic effect on the calculated power. At a constant flow rate, as the rotation rate increases, so does the calculated power. This results in a steeper trend as rotation rate increases. Figure 41 depicts the trend of the calculated efficiency versus flow rate over various rotation rates. The trend peaks around 72% efficiency for each rotation rate investigated, meaning that the rotation rate does not affect the peak efficiency. However, rotation rate does affect the volumetric rotation rate at which the peak efficiency occurs. A higher rotation rates moves the peak efficiency to a higher flow rate and vice versa.

Chapter 5

CONCLUSIONS

This investigation has shown that a person-portable micro-hydro power generation system is a numerically possible solution for remote power generation. This system will have military applications such as disaster relief scenarios as well as commercial applications such as power generation for remote locations.

Computational fluid dynamics packages such as the ANSYS line of products are an excellent numerical tool for this problem. A quality mesh with adequate solid-fluid interface resolution is vital for a good, physical numerical result. A transient analysis, using the renormalized-group analysis transport equations for turbulent flow and formulating the velocity scheme relative to a stationary runner, is ideal for the design analysis of the performance characteristics of this runner geometry.

Spectral and temporal convergence is a vital check to the validity of the numerical solution. It was shown that the medium sized mesh that was investigated is a good compromise between numerical accuracy and computational resources. The study also showed that the mesh and time-step selection of 100 time-steps per cycle is adequate enough to capture the important turbulent length scales for the determination of performance characteristics of the runner geometry.

Methods to attempt to capture the transient nature of the rotating impeller such as using a rotating mesh or rotating frame of reference correlate well between solutions. Their

differences in realizing the flow field are small. The rotating frame of reference appears to predict higher performance values than that of the rotating mesh, which is thought to be due to smoothing the transient nature of the flow with the rotating frame of reference.

The calculated head required to operate the turbine increases exponentially and is not really affected by rotation speed. The power generated is influenced more by the rotation speed than the required head, but still shows an exponential increase as flow rate increases. The calculated efficiency peaks around 72% efficiency no matter the chosen rotation rate, however, the rotation rate does determine which flow rate this peak efficiency occurs.

BIBLIOGRAPHY

[1] K. H. Fasol, "A Short History of Hydropower Control," *IEEE Control Systems Magazine,* pp. 68-76, August 2002.

[2] U. S. Department of the Interior, "The Hystory of Hydropower Development in the United States," Bureau of Reclamation, 1 August 2009. [Online]. Available: http://www.usbr.gov/power/edu/history.html. [Accessed 7 August 2012].

[3] G. Ingram, Basic Concepts in Turbomachinery, Ventus Publishing ApS, 2009.

[4] K. E. McCarthy, "Pros and Cons of Hydropower," Connecticut Office of Legislative Research, 4 October 2010. [Online]. Available: http://cga.ct.gov/2010/rpt/2010-R-0401.htm. [Accessed 7 August 2012].

[5] U.S. Department ofthe Interior, "Lowell Notes," *Experience Your America,* pp. 1-2, 30 October 2008.

[6] The American Society of Mechanical Engineers, "Kaplan Turbine," The American Society of Mechanical Engineers, York Haven, 1980.

[7] J. D. Anderson, J. Degroote, D. Gerard, D. Erik, R. Grundmann and J. Vierendeels, Computational Fluid Dynamics: An Introduction, 3rd ed., J. F. Wendt, Ed., Eagle River, WI: Springer, 2009.

[8] F. Frunzulica, I. C. Andrei, L. Sikolya and E. Korody, "Special Aspects in Triangulation and Mapped Meshing," Fascicle Mechanics, Tribology, Machine Manufacturing Technology, Baia Mare, 2005.

[9] J. P. Steinbrenner and J. R. Chawner, "Gridgen's Implementation of Partial Differential Equation Based Structured Grid Generation Methods," in *Proceedings of the 8th international Meshing Roundtable*, South Lake Tahoe, 1999.

[10] ANSYS, Inc., "Theory Guide," 2009.

[11] V. Yakhot and S. A. Orszag, "Renormalization-Group Analysis of Turbulence," *Applied and Computational Mathematics,* vol. 57, no. 14, pp. 1722-1724, 6 October 1986.

[12] V. Yakhot, S. A. Orszag, S. Thangam, T. B. Gatski and C. G. Speziale, "Development of turbulence models for shear flows by a double expansion technique," *American Institute of Physics,* vol. 4, no. 7, pp. 1510-1520, July 1992.

[13] ANSYS, Inc., "ANSYS 12.0 User's Guide," 2009.

[14] G. Iaccarino, "Predictions of a Turbulent Separated flow usig Commercial CFD Codes," *Journal of Fluids Engineering,* vol. 123, no. 4, pp. 819-828, 2001.

[15] J. Cadafalch, C. D. Perez-Segarra, R. Consul and A. Oliva, "Verification of Finite Volume Computations on Steady State Fluid Flow and Heat Transfer," *Journal of Fluids Engineering,* vol. 124, no. 1, pp. 11-21, 2002.

[16] Z. Liu and D. L. Hill, "Issues surrounding Multiple Frames of Reference Models for Turbo Compressor Applications," in *International Compressor engineering Conference*, West Lafayette, 2000.

[17] H. Nilsson and L. Davidson, "Validations of finite volume CFD against detailed velocity

and pressure measurements in water turbine runner flow," *International Journal for Numerical Methods in Fluids,* vol. 41, no. 8, p. 863–879, 200.

[18] P. M. Arenante, C. Luo, C.-C. Chou, I. Fort and J. Medek, "Velocity profiles in a closed, vessel: comparison betwen experimental LDV data and numerical CFD predictions," *Chemical Engineering Science,* vol. 52, no. 20, pp. 3483-3492, 1997.

[19] K. E. Morud and B. H. Hjertager, "LDA EASUREMENTS AND CFD MODELLING OF GAS-LIQUID FLOW IN A STIRRED VESSEL".

[20] J. Riglin, "Cavitation Study for a Microhydro Turbine," Lehigh University, Bethlehem, 2012.

VITA

W. Chris Schleicher graduated high school from Hempfield Area Senior High School in Hempfield Township, PA in 2007. He moved on to receive his Bachelor of Science Degree in Mechanical Engineering at York College of Pennsylvania in York, PA in 2011. He also had a co-operational opportunity with Voith Hydro in York, PA where he learned about CFD and the hydro turbine industry. He is currently studying at Lehigh University.